Astron. Astrophys. 65, 11—16 (1978)

ASTRONOMY AND ASTROPHYSICS

The Chromosphere above Sunspot Umbrae

I. Observations of the Emission Cores in the Ca II H- and K-Lines*

W. Mattig and F. Kneer

Fraunhofer-Institut, Schöneckstr. 6, D-7800 Freiburg, Federal Republic of Germany

Received July 15, 1977

Summary. Photographic spectra of the Ca II H- and K-lines in sunspot umbrae are analysed. The emission features in the line profiles may be classified into minimum emission profiles that also lack self-reversal, and profiles which change rapidly in time and exhibit self-reversals (umbral flashes) that are most often strongly asymmetric. Average intensity profiles from the minimum emission parts of the umbra and characteristic intensities of the more active parts of the umbra are given.

Key words: chromosphere — sunspot umbra — Ca II lines

1. Introduction

For an investigation of the quiet chromosphere one may observe both on the disc and beyond the limb (during eclipses) in both continua and spectral lines. An investigation of the chromosphere above sunspots has to rely solely on observations (for geometrical reasons on the disc) of strong Fraunhofer lines as long as sunspot observations of the chromospheric UV- and mm-continua with sufficient spatial resolution are not available. In this paper we present profiles of the Ca II H- and K-lines from sunspot umbrae. These lines are partly formed in the chromosphere and offer observational keys for the modelling of chromospheres (see e.g. Linsky and Avrett, 1970).

The central emission of H and K in sunspots has been known for a long time (Abetti, 1929). However, quantitative measurements started only with work of Mustel and Tsap (1960) and Engvold (1967). The latter author found as a common feature in sunspots a central K_3 absorption in the emission peak. This observation was not confirmed by Linsky (1970) and Shine and Linsky (1972). These authors, in addition, observe from different umbrae different values for the K/H intensity ratio: $I_{K3}/I_{H3} \approx 1$ in one umbra, which indicates an optically thick chromosphere, and $I_{K3}/I_{H3} \approx 1.7$ in another umbra, which indicates a thin chromosphere. Thus, it seems that the umbral chromosphere differs strongly from one sunspot to another. Moreover, we demonstrate in Figure 1 that sunspot chromospheres may exhibit fine structures in the H- and K-emission (see also Engvold and Livingston, 1969). Up to this time, most quantitative observations, including those of Teplitskaja and Efendieva (1973) and Teplitskaja and Firstova (1976), have been presented without regard to this fine structure in the umbra itself. Similarly, unresolved temporal variations, as for instance umbral flashes (Beckers and Tallant, 1969; Wittmann, 1969; Schultz, 1974), affect the significance of published "average" emission profiles.

The aim of this paper is to point out the importance of a careful inspection of the umbral area under investigation. In the following we select some parts of the umbrae which appear quiet and exhibit minimum emission in H and K. The line profiles from these areas may serve as a suitable basis for constructing static, at least stationary, chromospheric models of the "quiet" umbra with, hopefully, little disturbance by dynamic effects. Other parts of the umbra show strong activity and exhibit temporally variable, strongly asymmetric, and even self-reversed emissions in H and K as observed also by Beckers and Tallant (1969) and Schultz (1974). In these umbral regions time-dependent dynamic effects play probably the dominant role and should be taken into account when interpreting the observations.

2. Observations

The observations were made at the Schauinsland-observatory of the Fraunhofer-Institut. The primary lens of the tower telescope has an aperture of 45 cm, the scale at the spectrograph entrance amounts to $13'' \text{ mm}^{-1}$. The spectrograph is equipped with a 180×280 mm grating (632 rulings mm^{-1}) by PTR Optics Corp., the linear

Send offprint requests to: Dr. F. Kneer

* Mitteilungen aus dem Fraunhofer-Institut No. 153

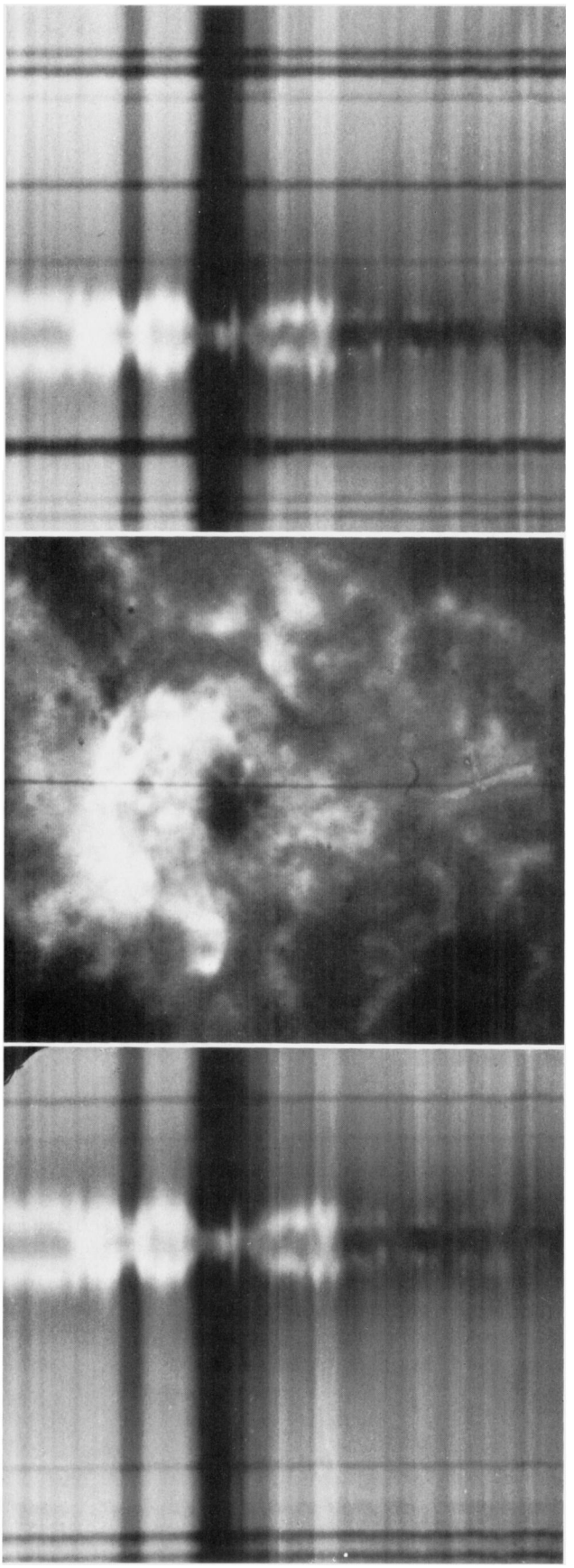

Fig. 1. An example of the chromospheric fine structure within the umbra of a sunspot

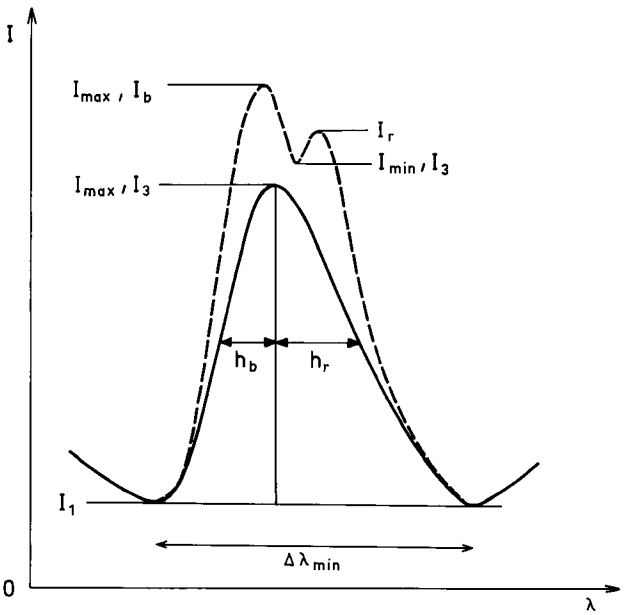

Fig. 2. Schematic emission profiles without self-reversal (full line) and with self-reversal (dashed line) for the definition of the notation

dispersion at H and K is 4.6 mm $Å^{-1}$ in sixth order. The H- and K-spectrograms were taken simultaneously with the same film (Agfa Pan 100, exposure time 7 and 20 s). The slit-jaw camera is equipped with a K-filter with 0.3 Å band width. A TV camera (SEC-Vidicon) monitors the K-image on a TV screen which is recorded on magnetic tape. The tape recording offers the extremely helpful possibility to check, after the event, the instrumental guiding performance and the seeing conditions during the relatively long exposure periods. K-filtergrams, for instance Figure 1, may be taken from the TV-screen.

For this paper we analysed spectrograms from a type H sunspot (Rome number 6544) on three consecutive days (1973 Sept. 2–4, position N 14 E 48-E 20). The diameter of the umbra was 16″. The guiding performance and the seeing conditions during the observations were approximately 1″ rms, that is, assuming a Gaussian spread function, the full width at half maximum was approximately 2″.4. The line profiles of H and K were measured across the sunspot with a microdensitometer; the densitometer data were transformed into intensities by means of the characteristic curve of the film. Then, the line intensities were scaled to the *photospheric* continuum intensity I_c. For this purpose we adopted for our observed photospheric intensities in the wings of H and K Linsky's (1970) calibrated values:

$$I_H(-1.3\,Å) = 0.133\,I_c \quad \text{and} \quad I_K(-1.3\,Å) = 0.165\,I_c .$$

The sunspot profiles were not corrected for scattered light. If seeing effects are negligible the influence of the straylight on the central parts of the emission cores is small because the line centre intensities in umbra and photosphere do not differ very much. At the position of the minima in the umbra profiles (H_1 and K_1) and in the

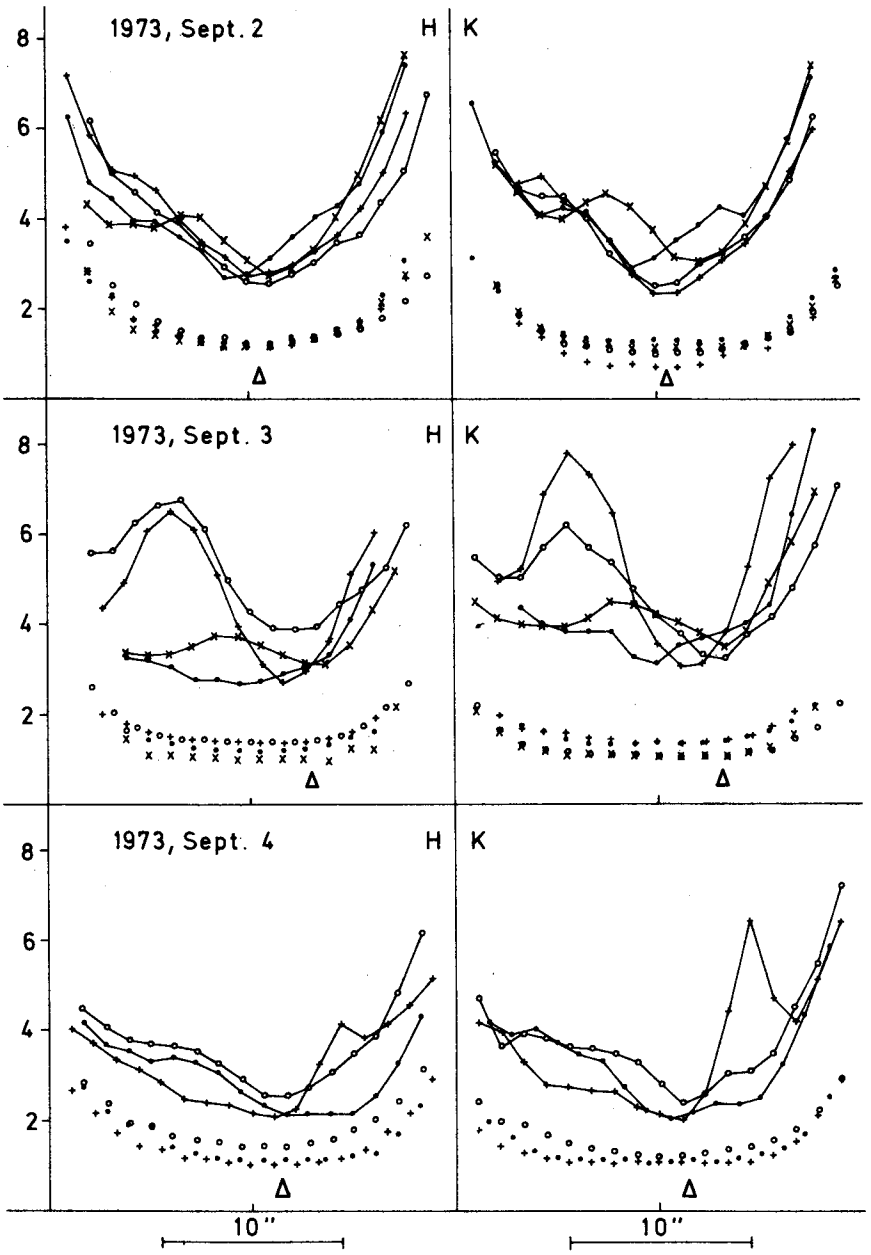

Fig. 3. H- and K-intensities in percent of the photospheric continuum intensity for two selected points in the line as a function of position and of time. Connected symbols: I_{max}; unconnected symbols: I_1. Sept. 2: ●$t=0$ s; ○$t=15$ s; $+t=40$ s; $\times t=55$ s. Sept. 3: ●$t=0$ s; ○$t=90$ s; $+t=230$ s; $\times t=270$ s. Sept. 4: ●$t=0$ s; ○$t=15$ s; $+t=300$ s

wings beyond H_1 and K_1 the influence of the scattered light may become large because the umbral and photospheric intensities differ by large factors. The scattered light correction should not alter the general appearance (small emission cores) of the umbral H and K profiles because the photospheric line intensities vary slowly with wavelength compared to the umbral profiles and the scattered light may be assumed, as a crude approximation, independent of wavelength. Then, an upper limit for the stray light intensity of about $0.01\,I_c$ may be estimated from the H_1 and K_1 intensities in the umbra which are of the same order in our observations (see below, Fig. 3).

3. Results and Discussion

For the sake of clarity we define first our notation of the features in the emission cores (see Fig. 2). We often omit the name of the line (H or K); it should be clear from the context to which line the given values belong. I_b and I_r refer only to the blue and red (resp.) maximum intensities in the self-reversed emissions. [Their usual designation in the literature is lengthy: $I_{K2b}(I_{H2b})$ and $I_{K2r}(I_{H2r})$.] A profile is defined to be self-reversed if at least a shoulder in the emission is clearly visible, i.e. if $I_b/I_{min}>1$ and $I_r/I_{min}\geqq 1$ or vice versa. I_{max} is the maximum intensity in the emission feature without regard to the presence of a self-reversal. I_{max}, I_3, I_{min}, I_b and I_r fall together if we see no self-reversal. The parameters h_b and h_r are the wavelength separations of the intensity at half maximum ($(I_{max}-I_1)/2$) from the position of I_3. Thus the full width at half maximum is FWHM $=h_r+h_b$ and the asymmetry is $A=(h_r-h_b)/(h_r+h_b)$. These two definitions are applied only to the pure emission peaks. I_1 is the mean value of the red and blue $K_1(H_1)$ intensities. In presenting our

results, we do not distinguish between the red and blue minimum intensity at $K_1(H_1)$ because of observational uncertainties in these parts of the lines.

a) Temporal and Spatial Variation of the Intensities

Figure 3 shows the variation of selected features in the line profiles across the umbra for the three different days. September 2 and 3 are represented by four spectrograms, consecutive in time, Sept. 4 is represented by 3 spectrograms. The connected points refer to the maximum emission peak intensity I_{max}, the unconnected points to the intensity at H_1 and K_1.

With regard to the maximum intensity I_{max} we notice: First, there exist large spatial intensity variations across the umbra (regardless of the intensity increase towards the penumbra). Second, I_{max} may show real variations with relatively short time scales. The Sept. 3 data show that locally limited variations by a factor of two (probably from umbral flashes) may occur within 90 s. Third, the intensity ratio $I_{max}(K)/I_{max}(H)$ is close to unity as long as no strong activity occurs. (See also the discussion of the "minimum emission" below.) This ratio may become larger during active periods (Sept. 4, crosses), thus indicating optically thin emission during these times. But this is not always the case. A contrary example is given in the Sept. 3 data (open circles) where the H emission seems on one occasion to be larger than the K emission. However, this case is anomalous since the whole line centre is brighter in H than in K which may signify an observational error.

Table 1. Characteristic data of "minimum emission" profiles

		Sept. 2	Sept. 3	Sept. 4	Average
I_1 [a]	H	1.23±0.01	1.41±0.19	1.23±0.15	1.29±0.17
	K	1.08±0.19	1.27±0.15	1.12±0.09	1.16±0.18
I_3	H	2.66±0.09	3.32±0.30	2.25±0.21	2.78±0.47
	K	2.68±0.28	3.42±0.18	2.23±0.19	2.82±0.53
$I_1(K):I_1(H)$		0.88±0.16	0.91±0.10	0.92±0.04	0.90±0.11
$I_3(K):I_3(H)$		1.01±0.08	1.04±0.13	0.99±0.01	1.02±0.09
FWHM	H	0.24 Å	0.19 Å	0.18 Å	0.21±0.03
(h_b+h_r)	K	0.25 Å	0.20 Å	0.19 Å	
Asymmetry	H	0.25	0.18	0.17	0.19±0.10
	K	0.11	0.36	0.08	
$\Delta\lambda_{min}$	H	0.68 Å	0.71 Å	0.65 Å	0.69±0.03
	K	0.68 Å	0.74 Å	0.68 Å	

[a] Intensities in percent of the photospheric continuum, for definitions see Figure 2 and text

b) Minimum Emission

One of our aims is, as already mentioned, to examine the umbra for regions with minimal temporal variation which may reasonably be called the quiet umbra. We feel that observations of the H- and K-line profiles from these parts should be interpreted first, before the problem of explaining time variations on small spatial scales is attacked. On the basis of the material there do appear to be regions with very little temporal fluctuation indicated by "arrows" in Figure 3. It happens that the profiles from these regions show pure emission peaks, without self-reversal.

The characteristic data of the minimum emission profiles are given in Table 1. The line profiles themselves are plotted in Figure 4. The variations from day to day, especially of the maximum intensity I_3, exceed the observational uncertainties and must be due to real, secular, changes in the umbral chromospheric structure. The intensity ratio $I_3(K)/I_3(H)$ is close to unity which indicates emission from an optically thick chromosphere.

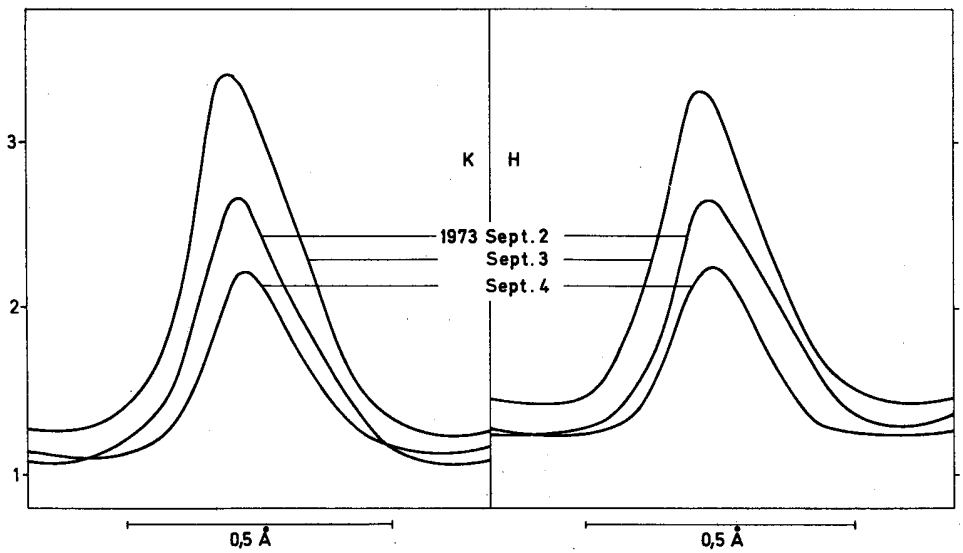

Fig. 4. Average H- and K-line profiles from the quiet umbrae; intensities I_λ in percent of the photospheric continuum intensity

It is also worth noticing that the profiles are always asymmetric in one direction, that is, with respect to the red and blue $K_1(H_1)$ minima, the position of $K_3(H_3)$ is shifted towards shorter wavelengths. This appearance could be due to differential velocities in the umbra itself. However, the influence of scattered light cannot be ruled out: If the scattered light varies asymmetrically across the line it induces asymmetry in the umbral line profile. Observations with the best possible scattered light corrections are urgently needed and are planned for the near future.

c) Self-Reversals

As Engvold (1967) had found, the self-reversal of the emission peaks is the normal behaviour in umbrae, though the separation of the K_2 peaks is much smaller than in the quiet chromosphere and in plages. We investigated the occurence of the self-reversal in our observations. It is plotted in Figure 5 for the K-line; the H-line behaves almost identically. Average intensity ratios are given in Table 2.

We may summarize the result as follows: In the central parts of the umbrae (within a radius $r \leqq 5''$) 43 out of the 198 investigated profiles show a central K_3-absorption. It is important to note that all umbral flashes have self-reversed profiles, but extremely asymmetric ones with a strong blue emission and only faint red emission ($I_b \gg I_r$). If we exclude the umbral flashes 24 profiles exhibit self-reversals.

Outside the central parts of the umbra ($r > 5''$) the K_3 absorption occurs more frequently and with an appearance already known from Engvold's (1967) observations at the penumbra border.

In almost all cases of self-reversal the blue emission peak is higher than the red one. Only 5% of the self-reversed profiles have $I_b < I_r$.

Within the observational errors the wavelength separation $\Delta\lambda$ of the emission peaks is the same for *H* and *K*. Without the umbral flashes we obtain a mean value of $\Delta\lambda = (0.10 \pm 0.03)$ Å. For the umbral flashes alone we measure a larger separation: $\Delta\lambda = (0.14 \pm 0.04)$ Å.

4. Conclusion

The above investigation revealed several observational needs for sunspot chromospheres: First, high spatial resolution is necessary in order not to mix too different types of profiles into an average profile. Second, the lines of interest should be observed *simultaneously* and within a short time period because of the possibility of rapid changes of the chromospheric structure. Most previous observations do not fulfill the two above requirements. Third, time series with high temporal resolution and a long duration are desirable in order to check the concept of the quiet and active umbra. And fourth, much work needs to be done with the stray light problem. Otherwise such observational features as the asymmetry and the true intensity at H_1 and K_1 remain too uncertain to yield valuable information on the umbral structure.

As already mentioned, we introduced the concept of the quiet and active umbral chromosphere: Profiles from the quiet part have minimum emission without self-

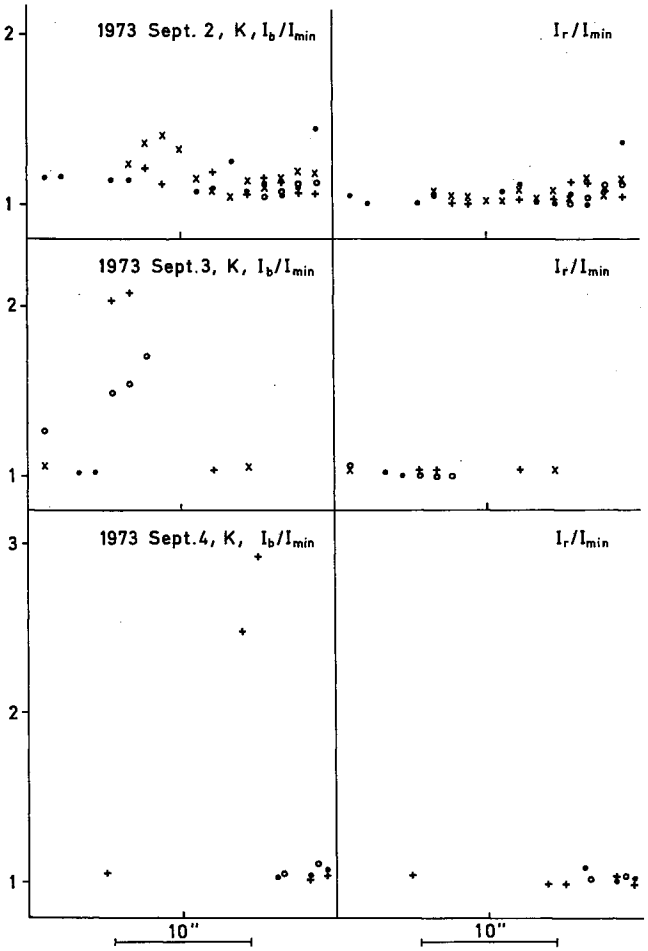

Fig. 5. Occurrence of self-reversed emission profiles as a function of position and time. Intensity ratios of the blue and red emission to the central absorption in the K-line are given. (For notation see Figure 2. The designation of the points for different times is the same as in Figure 3)

Table 2. Intensity ratios in self-reversed emission cores

		H	K
Central part of umbra (10") without umbral flashes	$I_b:I_{min}$ [a]	1.12±0.05	1.12±0.08
	$I_r:I_{min}$	1.06±0.06	1.03±0.03
Outside central part	$I_b:I_{min}$	1.12±0.05	1.10±0.06
	$I_r:I_{min}$	1.06±0.06	1.05±0.03
Umbral flashes alone	$I_b:I_{min}$	1.75±0.51	1.77±0.54
	$I_r:I_{min}$	1.01±0.02	1.02±0.02
Red peak stronger than blue peak	$I_b:I_{min}$	1.03	1.02±0.02
	$I_r:I_{min}$	1.05	1.06±0.02

[a] For definitions see Figure 2

reversal, the intensity ratio I_{K3}/I_{H3} is close to unity. Profiles of an active umbral chromosphere show rapid changes in time and possess a self-reversal which is often very asymmetric.

With such a distinction, the problem of interpreting at least the quiet umbral profiles should be simplified.

Certainly, the validity of this concept needs further observational proof, or disproof, since the time sequences used for this investigation were neither complete nor very long.

Acknowledgements. It is pleasure to thank Dr. C. J. Durrant for discussions and helpful comments.

References

Abetti, G.: 1929, Handb. d. Astrophysik, IV, 57
Beckers, J.M., Tallant, P.E.: 1969, *Solar Phys.* **7**, 351
Engvold, O.: 1967, *Solar Phys.* **2**, 234
Engvold, O., Livingston, W.: 1969, *Publ. Astron. Soc. Pacific* **81**, 195
Linsky, J.L.: 1970, *Solar Phys.* **11**, 355
Linsky, J.L., Avrett, E.H.: 1970, *Publ. Astron. Soc. Pacific* **82**, 169
Mustel, E.R., Tsap, T.T.: 1960, *Isv. Krymsk. Astrof. Obs.* **22**, 75
Schultz, R.B.: 1974, NCAR Cooperative Thesis No. 32, University of Colorado
Shine, R.A., Linsky, J.L.: 1972, *Solar Phys.* **39**, 49
Teplitskaja, R.B., Efendieva, S.A.: 1973, *Solar Phys.* **28**, 369
Teplitskaja, R.B., Firstova, N.M.: 1976, *Solar Phys.* **48**, 403
Wittmann, A.: 1969, *Solar Phys.* **7**, 366

Astron. Astrophys. 65, 17–28 (1978)

ASTRONOMY AND ASTROPHYSICS

The Chromosphere above Sunspot Umbrae.

II. The Interpretation of the H, K, and IR Lines of Ca II*

F. Kneer and W. Mattig

Fraunhofer-Institut, Schöneckstr. 6, D-7800 Freiburg, Federal Republic of Germany

Received July 15, 1977

Summary. The chromospheres above sunspot umbrae are investigated by comparing calculated and observed profiles of the Ca II H, K, and infra-red lines. Statistical steady state is assumed for the level populations. We test several model chromospheres in hydrostatic equilibrium. We distinguish between chromospheres which are optically thick and optically thin at the centre of the K line. In view of the observed intensity ratio $I_{K3}/I_{H3} \approx 1.15$ we are forced to adopt a thick model as reference chromosphere.

Key words: chromosphere — sunspot umbra — Ca II lines

1. Introduction

The spectra of sunspot umbrae show emission cores in the Ca II H and K lines. This indicates that the radial temperature profile above a sunspot passes through a minimum: in other words, that umbrae possess chromospheres (Linsky and Avrett, 1970).

With regard to the energy balance of sunspots Biermann (1941) suggested that the convective energy transport is largely *prohibited* by the magnetic field and that therefore sunspots are cooler than the normal photosphere. Danielson and Savage (1968) discussed whether the missing flux in sunspots could be carried by magneto-acoustic waves. In contrast to the Biermann picture, Parker (1974) proposed that sunspots are regions of *enhanced* energy transport in the form of Alfvénic flux so that as a net effect the umbral material is cooled. A study of the structure and dynamics of the atmosphere above sunspots should help choose between these two very different points of view (Beckers, 1976; Foukal et al., 1974).

The question of energy balance in sunspots is interesting in its own right, but in addition we can learn a great deal by comparing and contrasting the chromospheres of sunspots with the chromosphere of the quiet sun. Since we know that the magnetic pressure in sunspots is comparable to—or larger than—the gas pressure we expect the magnetic field to influence the energy transport and dissipation mechanisms (Marik, 1967) and to produce chromospheres very distinct from the ones of the quiet regions without magnetic fields. Thus, we can think of the two types of atmospheres, umbral and quiet chromospheres, as two nearby stellar laboratories with different —only partly understood—equipment.

On these grounds it is important to know the structure of both types of chromospheres. However, while an enormous number of investigations of the quiet chromosphere and its fine structure have been undertaken, very little work has been devoted to the umbral chromosphere. The reason for the underrepresentation of research in this field is obvious: both observational and interpretational difficulties far surpass the problems met in studies of the quiet chromosphere. Observationally, the high intensity radiation from the ambient area on the sun falsifies the true umbral radiation through atmospheric and instrumental scattering of light and through seeing effects. In the far ultra-violet region the spot emission seems to be comparable to the emission from the surrounding medium so that false light plays a minor role (Foukal et al., 1974; Cheng et al., 1976). However, observations in this spectral region with high spatial and wavelength resolution have become available only in the last few years. Interpretationally, our ability to treat non-LTE line formation in magnetic fields has only recently improved (Omont et al., 1973; House and Steinitz, 1975; Auer et al., 1977).

Despite these difficulties we feel that it is possible to use existing observations to draw some conclusions on the structure of umbral chromospheres, at least as a starting approximation. We use here as diagnostic probes only the five strongest lines of Ca II. The next section is devoted to the observational data of these lines. Section 3 deals with the assumptions and numerical methods concerning the treatment of both the model atmosphere and the Ca

* Mitteilungen aus dem Fraunhofer-Institut No. 150

atom. In Section 4 we discuss several models and compare them with results of other investigators.

2. Observations

We do not present new observations here, but rather collect some prominent observational features of the Ca II H, K and IR lines. It is important to notice here that we are not able to give exact figures of calibrated observations for two reasons. First, sunspot structure differs from one spot to another and sunspots exhibit a variety of different profiles of the same line. Second, as already mentioned, the observed spot intensities are falsified by scattered light whose influence may be seen from the following formula (Zwaan, 1965)

$$I' = (1 - \beta)I + \beta I^a. \quad (1)$$

Here, I and I' are the true and observed spot intensities, respectively, βI is the fraction of light scattered *out* of the beam and βI^a is the fraction of light scattered *into* the beam from the ambient area. We see at once from Equation (1) that for equal intensities in spot and surrounding area ($I = I^a$) the scattering has no influence. On the other hand, it follows for (relatively) small sunspot intensities ($I \ll I^a$) that the observed intensities are strongly falsified. Usually (Kneer, 1972), the continuum intensity ratio of sunspot to photosphere *decreases* towards shorter wavelengths (in the visible spectral range), while the fraction of scattered light *increases*. As a consequence, at a continuum wavelength near the H and K lines, the false light may override the weak intensity from the spot. From this discussion we learn to accept observed sunspot line profiles with caution.

With the above in mind we summarize the relevant properties of the H, K, and IR lines in sunspots in Table 1. The first column of Table 1 indicates the spectral feature, the second column its behaviour, and the third column the sources. Most of the figures refer to observations close to the disc centre. We exclude such prominent observational facts as brightness and velocity oscillations (Beckers and Tallant, 1969; Beckers and Schultz, 1972) and line asymmetries (Teplitskaja and Firstova, 1976). We concentrate in this paper on the interpretation in terms of time independence: the modification of the

Table 1

H and K lines:		
I_{K3}	$0.5 \cdots 1.0 \times I^{\odot}_{K3}$*	M, E, L, SL
	$\approx 0.5 \cdots 1.0 \times 10^{-6}$ erg cm^{-2} s^{-1} sterad^{-1} Hz^{-1}	
self-reversal?	yes	E, TEa (near limb)
	($I_{K2} \approx I_{K3}$, self-reversal small, $\Delta\lambda_{K2} \approx 0.06$ Å	E
	no	MK, L, SL, MT
I_{K1}	$0.1 \cdots 0.3 \times I_{K3}$	MK, L, E, SL, MT
$\Delta\lambda_{K1}$	$0.25 \cdots 0.35$ Å	MK, L, E, SL, MT
FWHM**	$0.2 \cdots 0.25$ Å	MK, TEb
wings beyond K_1	flat compared to wings in plages	MT
I_{K3}/I_{H3}	$1.0 \cdots 1.3$	MK, L, TF
	1.7	SL
I_{K1}/I_{H1}	$\lesssim 1.0$	MK, L, SL
IR lines:		
emission cores?	no! pure absorption lines	
residual intensities at line centre	~ 0.25	
relative intensities at line centre	$I_{8498} > I_{8542} > I_{8662}$	SL
relative intensities in wings	$I_{8498} > I_{8662} > I_{8542}$	

Sources: E: Engvold (1967); L: Linsky (1970); MK: Mattig and Kneer (1977); MT: Mustel and Tsap (1960); SL: Shine and Linsky (1972); TEa: Teplitskaja and Efendieva (1971); TEb: Teplitskaja and Efendieva (1973); TF: Teplitskaja and Firstova (1976)

* $I^{\odot}_{K3}$ is the intensity measured from the quiet chromosphere

** FWHM = full width at intensities $(I_{K3} + K_{K1})/2$. K_1 is the minimum in the line profile

resulting models by a dynamic interpretation will be an important future step.

Let us comment briefly on some items of Table 1: The intensity of the centre of the K line, I_{K3}, is only weakly contaminated by scattered light because it differs only little from the intensity of the quiet chromosphere, $I^{\odot}_{K3}$. We can estimate the latter by comparing the measurements of White and Suemoto (1968) with the continuum intensity at 4000 Å calculated from the Harvard Smithsonian Reference Atmosphere (Gingerich et al., 1971), which is in good agreement with the calibrated observations of Labs and Neckel (1968). From this one is led to $I^{\odot}_{K3} \approx 1.0 \times 10^{-6}$ erg cm^{-2} s^{-1} sterad^{-1} Hz^{-1} at disc centre. Linsky (1970) and Shine and Linsky (1972) present their line profiles with respect to the local continuum in the umbra. If we admit that, due to false light, their continuum intensities at the K line are too high by possibly 10 to 50 percent we may conclude from their data that the continuum and line centre intensity are approximately equal in the spot. Reasonable umbra models of the continuum emitting layers (see Section 4) give values of $I_{\rm cont} \approx 6.0 \times 10^{-7}$ erg cm^{-2} sterad^{-1} = $0.6 I^{\odot}_{K3}$. This is in line with the results of other observers. (See Linsky and Avrett, 1970, for a similar estimate of the K_3 intensity in sunspots.)

We defer comments on the question of the self-reversal to the discussion of our models (Section 4). The intensity of K_1 (H_1) and also the wing intensities beyond K_1 may be affected by false light and most of the published values are probably too high by some 10 to 50 percent. However, the flat damping wings of the K line, as shown to a distance of about 3.5 Å from line centre in the observations of Mustel and Tsap (1960), are worth noticing. The intensity ratio I_{K3}/I_{H3} will turn to an important diagnostic tool for the investigation of the thickness of the umbral chromosphere and will also be discussed in Section 4. The position of the K_1 minimum in sunspots is reported consistently by many observers. Possibly, it is only little influenced by scattered light.

The only observations of the IR lines available to us are those of Shine and Linsky (1972). Unfortunately, as they themselves state, their data contain contributions from the surrounding penumbra and plage regions because of poor seeing conditions. We take for granted that we are dealing with pure absorption profiles. Unless contradictory observations turn up this is an additional observational constraint for modelling chromospheres above sunspots. Clearly, there is a pressing need for more observations of these lines.

3. Assumptions and Methods

In this section we outline the several assumptions and methods used here for the modelling of chromospheres and for the calculation of both the ionization equilibrium of the calcium atom and the emergent line profiles.

3.1. Hydrostatic Equilibrium

For each model atmosphere we specify a one-dimensional run of temperature $T(p_{\rm tot})$ as a function of total pressure $p_{\rm tot}$ or, equivalently, of column mass density m by means of the equation for hydrostatic equilibrium

$$p_{\rm tot} = gm \tag{2}$$

where g is the surface gravity acceleration. At the upper boundary, for $m = 0$, we have put $p_{\rm tot} = 0$. The column mass density is related to the mass density ρ and geometric height h through

$$dm = -\rho dh. \tag{3}$$

For many needs one is forced to calculate the mass density ρ as a function of the temperature and the electron density n_e. The latter is an implicit function of abundances, temperature, gas pressure p_g, and radiation fields J_ν at all frequencies ν, which influence the ionization equilibrium within the gas:

$$F(n_e, \varepsilon_i, T, p_g, J_\nu) = 0. \tag{4}$$

We use the same chemical composition as in the Kitt Peak code (subroutine STATE) of Auer et al. (1972), including calcium as an additional electron donor at low temperatures. This code treats the formation of the H_2 and H_2^+ molecules and the ionization of the metals, He, and H^- in LTE. The non-LTE ionization of hydrogen is discussed below. With a known functional or numerical dependence of the ionization equilibria on n_e, T, and p_g we solve Equation (4) iteratively for n_e by a secant method.

3.2. The Ionization of Hydrogen

For the non-LTE deviation factor b_1 of the hydrogen ground level we adopt an analytic approximation due to Kalkofen (quoted by Linsky, 1968)

$$1/b_1(\tau_0) \approx G[1 + (\sqrt{\varepsilon_0} - 1) \exp(-\sqrt{3\varepsilon_0}\tau_0)], \tag{5}$$

where τ_0 is the optical depth at the head of the Lyman continuum. The above formula is an extension from a treatment by Dietz and House (1965) of a ground level plus continuum hydrogen atom to an inclusion of the second bound level with Ly-α in detailed radiative balance. Thus, ε_0 is essentially the ratio of collisional to radiative recombination to the ground level and G is a correction factor which accounts for radiation and collision processes to the second bound level. (The reader is referred to the Appendix for the detailed expressions of ε_0 and G.) The factor $\sqrt{3}$ in the exponent is a consequence of the Eddington approximation.

Except for the mean radiation field in the Balmer continuum only local quantities (n_e, T, τ_0) enter into the right-hand side of Equation (5). The intensity of the

Balmer continuum may be specified by a radiation temperature $T_{R,B}$ by the choice of a special column mass density m_0 in such a way that

$$T_{R,B}(m) = T(m) \quad \text{for } m > m_0,$$

and

$$T_{R,B}(m) = T(m_0) \quad \text{for } m < m_0.$$

The choice of m_0 is difficult because no calibrated observations of the Balmer continuum in sunspots are available. One preliminary choice of m_0 could be the point in the atmosphere where the head of the Balmer continuum has an optical depth of about unity. We believe that this point lies deeper in the atmosphere than the temperature minimum. We usually choose m_0 at $T = 3500$ K; we discuss the influence of $T_{R,B}$ in the next section. With the specification of $T_{R,B}$ it is possible to treat the hydrogen ionization as an initial value problem with $\tau_0 = 0$ at the top of the atmosphere.

The main assumption underlying the approximate formula (5) is that none of the parameters vary with height; this is equivalent to the assumption of an isothermal atmosphere with constant density and constant $T_{R,B}$. Certainly, real atmospheres need a more detailed treatment of the radiation fields, but we wish to defer a more consistent calculation of the hydrogen ionization to a future investigation when, hopefully, observational data of the Ly-α line, the Ly-continuum, and the Balmer continuum in sunspots will be available. We apply the above formula because it provides a better approximation than LTE for the contribution of hydrogen to the electron density where deviations from LTE are important. According to our experience, Equation (5) leads to electron densities in quiet chromospheric models with an accuracy of 50 percent or better compared with self-consistent non-LTE calculations.

3.3. *The Ionization of Calcium*

(a) The Ca II/Ca I Density Ratio

A self-consistent determination of the ratio of the Ca II to Ca I densities has to account for many collisional and radiative transitions (Linsky, 1968). We avoid this difficult task by assuming that Ca I is ionized in LTE. For this purpose we adopt from Linsky (1968) an ionization energy for Ca I of $\chi_I = 6.11$ eV and a ratio of the partition functions at low temperatures of $U_{II}/U_I = 2$. Table 2 gives the density ratio if Ca II to Ca I for some heights near the temperature minimum in one of our models. We see that even near the temperature minimum the Ca I density is less than 25 percent of the total Ca density. We may argue as follows that this is probably an overestimate: Below a temperature of 4000 K dielectronic recombinations do not seem to play the dominant role in populating the Ca I atom (Burgess, 1965), so that photoionizations and -recombinations are probably the important processes determining the Ca II/Ca I density ratio. Then, since the ionizing radiation fields at the temperature minimum usually originate in deeper layers corresponding to a higher radiation temperature, the levels of the lower ionization stage tend to be depopulated at a higher rate than under LTE conditions. (See for instance the behaviour of the ground level deviation factor of hydrogen at the *photospheric* temperature minimum in the model of Vernazza et al., 1973.) We thus conclude that a more detailed treatment of the Ca II/Ca I density ratio would have little influence upon our conclusions regarding the line profiles of Ca II.

Table 2

m (g cm^{-2})	T (K)	$n_{\mathrm{Ca\,II}}/n_{\mathrm{Ca\,I}}$
0.01	3350	102
0.0315	3200	26
0.1	3200	12
0.315	3250	6.7
1.0	3390	5.7
2.14	3480	5.0
4.57	3600	4.8
10	3820	6.2

(b) The Ca II–Ca III Level Populations

We next consider our model representation of the Ca II ion of Figure 1. Only the five lowest levels plus the continuum (Ca III) are included. For test calculations we will restrict the model ion further, to levels 1, 3, 5, and 6; this is a fair representation according to Linsky (1968) and to our experience with low temperature atmospheres. The atomic data used in this investigation are given in the Appendix.

It is our aim in this investigation to study the line profiles of the five strongest Ca II lines emerging from model atmospheres. For this purpose we assume a statistical steady state for the level populations. The steady state equations and the radiative transfer equations in *one*-dimensional geometry are simultaneously solved with the complete linearization method in the form worked out by Auer and Heasley (1976). In this scheme the first-order corrections to the *radiative rates* are computed, and this is superior to calculating corrections to the *radiation fields* when many broad lines are to be treated. The influence of the magnetic field is excluded and deferred to a forthcoming investigation.

We treat only *line* transitions in detail. The photoionization rate coefficients are kept fixed for each model atmosphere by specifying a radiation temperature similar to the Balmer radiation temperature in the hydrogen

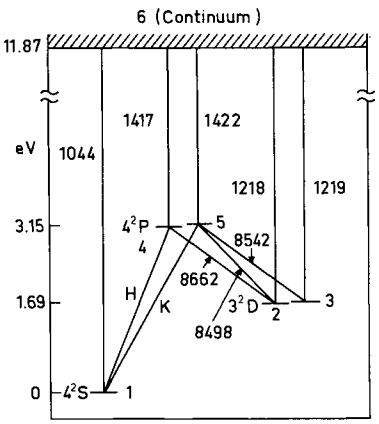

Fig. 1. Energy level diagram of Ca II and radiative transitions

ionization problem. Such a procedure causes uncertainties in our calculations of the level populations because of the lack of observations of the ionization continua of Ca II below 1422 Å in sunspots. However, some guidance can be obtained by the height of formation of the background continua, essentially the C I continua at 1444 Å, 1239 Å, and 1100 Å, in the quiet chromosphere. According to Vernazza et al. (1973), these are formed between 750 km and 1200 km, at pressures of roughly 8 to 200 dyn cm^{-2}. Assuming that carbon is mainly neutral in this layer in both sunspot and quiet chromosphere we obtain with Equation (1) column mass densities of about 3×10^{-4} to 7×10^{-3} g cm^{-2} as bounds to the region where the background continua are becoming optically thick. As standard values we choose the points $m_0 = 10^{-3}$ g cm^{-2} for the continua from the 4 *S* and 4 *P* levels of Ca II and $m_0 = 5 \times 10^{-3}$ g cm^{-2} for the continua from the 3 *D* levels of Ca II. Deeper in the atmosphere the radiation temperature follows the electron temperature ($T_R = T$), higher up it is supposed to be constant ($T_R = T(m_0)$). We shall discuss the influence of these radiation temperatures on the ionization equilibrium and the line formation in Section 4.

3.4. Absorption and Emission Profiles

As already mentioned, the splitting of the lines due to a magnetic field in sunspots of possibly 2000 to 3000 Gauss will be investigated in a forthcoming study and is not taken into account here. As absorption profile we use the normalized Voigt function

$$\phi(v) = \frac{1}{\sqrt{\pi}} H(a, v), \tag{6}$$

where a and v have their usual meaning.

It was shown by Shine et al. (1975) that a treatment of the Ca II, H and K lines by means of partial redistribution (PRD) is by far better than the assumption of equality of emission and absorption profiles or complete redistribution (CRD). Since PRD strongly influences the wings of the lines and the intensity ratio of the H and K lines we have to use PRD models to study, for example, the position of the K_1 minima. For this purpose we use the formalism by Heasley and Kneer (1976); as suggested by the results of Shine et al. (1975), we treat only the H and K lines with PRD and assume CRD for the IR lines. For simplicity the approximate form of the redistribution function R_{II} by Jefferies and White (1960) is adopted and normalized as proposed by Kneer (1975). Since the complete linearization scheme of Auer and Heasley (1976) does not allow for the linearization of a line source function depending explicitly on the radiation field we lag the PRD calculations behind each linearization cycle, i.e. we only partially linearize the radiative transfer equation. This procedure was recommended by Heasley and Kneer (1976) and it does not deteriorate the convergence properties of the scheme in the case of the Ca II ion.

4. Umbra Models

4.1. Temperature, Electron Density, and Macro-Velocity

In Figures 2 and 3 the run of temperature, electron density, and mass density of four umbra models is given. The corresponding heights are also indicated at the bottom of Figure 2. ($h = 0$ at $\tau_{5000} = 1$.) The temperature model in the deep layers below the 3200 K level is taken from Kneer (1972). The difference between the latter model and models by Hénoux (1969) and Stellmacher and Wiehr (1970) is of little influence on the discussion of models of umbral *chromospheres*. The 3200 K minimum is somewhat uncertain: the available observations of the Ca II lines determine the temperature in these layers within about ± 400 K. Only temperatures below 12 000 K are given. Our actual models extend almost linearly on the logarithmic mass scale to 16 000 K. The chromospheres *A*, *B*, and *C* qualify as optically *thick* in the centre of the K line. Model *D* is optically *thin*. We comment on this below.

Figures 4 and 5 show calculated profiles near the core of the H, K and IR lines at $\cos\theta = 0.89$. The profiles of Figures 4 and 5*a,b,c,d* correspond to the models *A*, *B*, *C*, and *D*, respectively. The micro-velocity used in these calculations (except for Figs. 4*d* and 5*d*) is 1 km s^{-1} throughout the atmosphere; this seems to be an upper limit in the deep layers according to Kjeldseth Moe (1973). (The weakly drawn H and K lines in Fig. 4*d* and the IR lines in Fig. 5*d* are calculated with the micro-velocity of Fig. 7, curve 4.)

Only the thin model *D* produces non-reversed emission cores in H and K. The reason may be seen in Figure 6, which displays the line centre K line source functions and the corresponding Planck function versus τ_{0K} (the

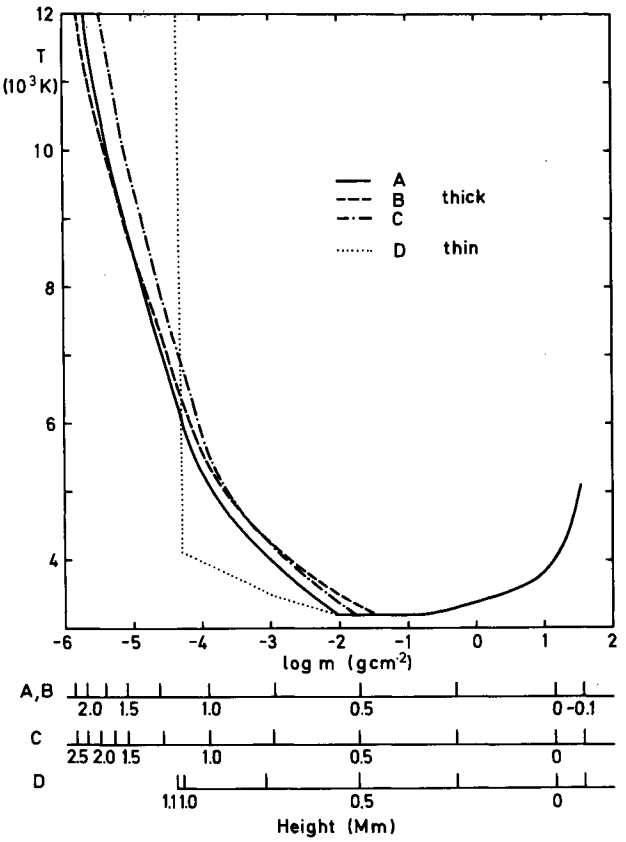

Fig. 2. Temperature versus column mass density for models 1 to 4. Bottom: geometric height for the different models; $h = 0$ at $\tau_{5000} = 1$

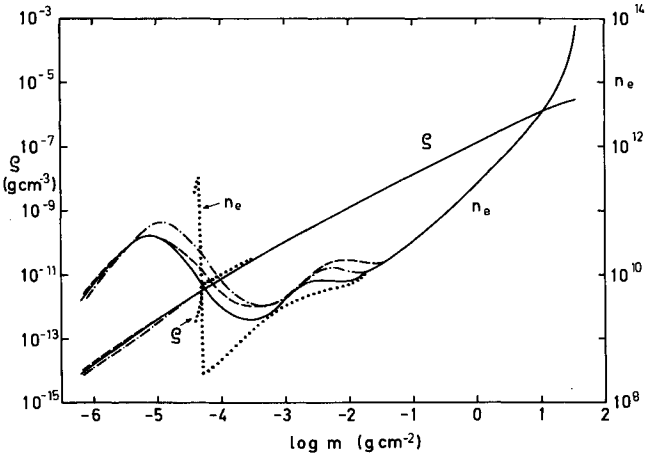

Fig. 3. Electron density (particles per cm³) and mass density versus column mass density for model *A* (full line), *B* (dashed), *C* (dash-dotted), and *D* (dotted)

line centre optical depth in the K line) for the four models. While the thick models have their source function maxima in the range $10 \lesssim \tau_{0K} \lesssim 20$ and so produce self-reversed emission cores, the source function maximum in the thin model is situated where $\tau_{0K} < 1$, leading to a simple emission core.

Athay and Skumanich (1968) suggested that the observed absence of self-reversal in sunspot K line profiles was an indication that the chromosphere above sunspots is optically thin in the K line. Optically thin models are tightly constrained by the requirement that the source function maximum lies where $\tau_{0K} < 1$, i.e. that the main contribution to the emission comes from optically thin layers. This is only possible when there are high electron densities at high temperatures in these layers. The high temperature electrons provide a large thermal source for photons through collisional excitation and subsequent spontaneous radiative emission. In a two-level atom approximation, the total emission E is proportional to the cumulating effect of collisional excitation

$$E \propto \int C_{lu} dn_{\mathrm{Ca\,II},l} \tag{7}$$

where C_{lu} is the collisional rate coefficient from the lower to the upper level and $n_{\mathrm{Ca\,II},l}$ is the density in the ground

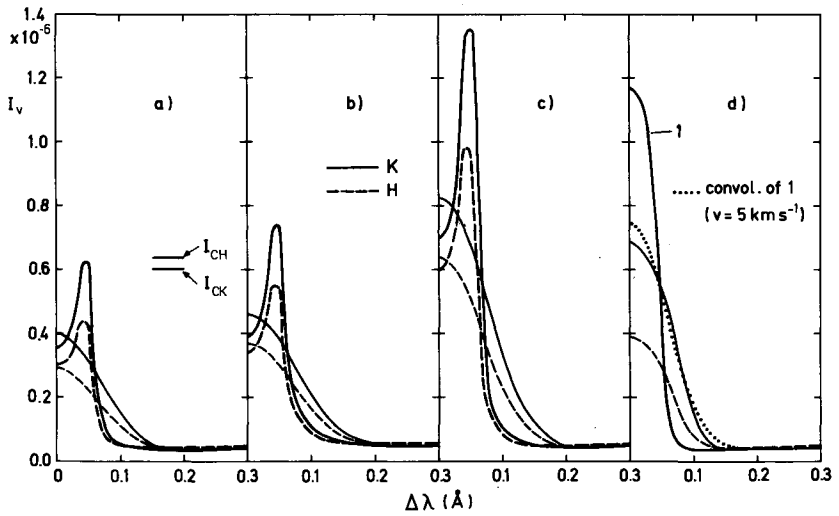

Figs. 4a–d. Emergent intensities of H and K lines at $\cos\theta = 0.89$ in absolute units (erg cm^{-2} s^{-1} sterad^{-1} Hz^{-1}) versus distance from line centre in Å for models *A* (a), *B* (b), *C* (c), and *D* (d). I_c = continuum intensity, equal for all models. (a), (b), and (c): heavily drawn profiles: $v_t = 1$ km s^{-1}; weakly drawn profiles: convolution of heavily drawn profiles with Gaussian distribution corresponding to a velocity amplitude of $v_{\mathrm{macro}} = 5$ km s^{-1}. (d): profile labelled 1: K line, $v_t = 1$ km s^{-1}; dotted: convolution of 1 with Gaussian distribution $v_{\mathrm{macro}} = 5$ km s^{-1}; weak lines: H and K calculated with run of micro-turbulence according to Figure 7, curve 4. Micro- and macro-turbulence have nearly the same effect on the line profiles from the thin model *D*

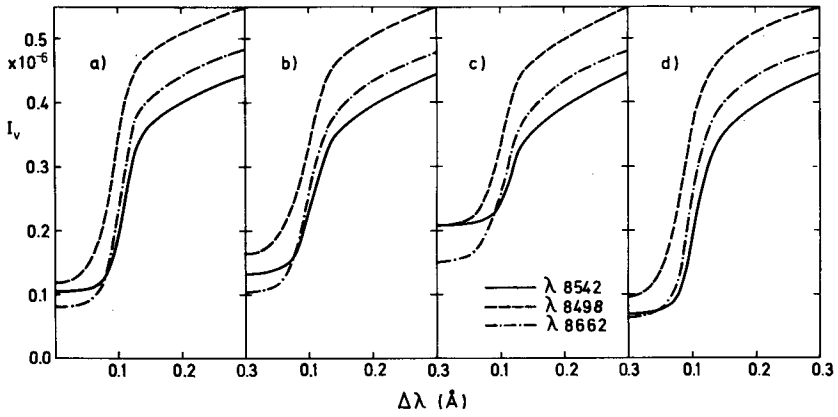

Fig. 5. Emergent intensities of the IR lines at $\cos\theta = 0.89$ in absolute units for the models *A* to *D*. (a)–(c): $v_t = 1$ km s^{-1}; (d) v_t according to curve 4 of Figure 7.

$I_{c\,8542} = 7.53 \times 10^{-6}$ erg cm^{-2} s^{-1} sterad^{-1} Hz^{-1};

$I_{c\,8498} = 7.48 \times 10^{-6}$ erg cm^{-2} s^{-1} sterad^{-1} Hz^{-1};

$I_{c\,8662} = 7.70 \times 10^{-6}$ erg cm^{-2} s^{-1} sterad^{-1} Hz^{-1}

level of Ca II. To the same approximation, the proportionality (7) can be expressed as

$$E \propto \int \varepsilon B d\tau_K \qquad (8)$$

where $\varepsilon \approx C_{ul}/A_{ul}$ with the Einstein coefficient A_{ul}, and B is the Planck function. The integral has to be taken over the optically thin emitting layer. Neglecting the coupling collisions between the upper levels of the H and K line transitions, we may apply the same Equation (8) with the same ε and B to the H line except that the latter has half of the opacity of K ($d\tau_H = \frac{1}{2}d\tau_K$). Thus, one would expect an intensity ratio in the emission cores close to 2. The thin model *D* gives $I_{K3}/I_{H3} = 1.77$. Such a large value has been observed only once, by Shine and Linsky (1972). If the electron density and the temperature do not drop *rapidly enough* towards larger optical depths in the *K* line the cumulating effect of thermal sources leads to an increase in the line source function towards larger optical depth, and this produces a self-reversal in the emission.

Thus, except for very special models, thin models will exhibit intensity ratios which are too large, while thick models will exhibit central reversals. It seems improbable that sunspots always produce those special atmospheres (we have not found one) which are thick enough to reduce the intensity ratios, but not too thick to lead to self-reversal. This argument does not rely on the assumption of hydrostatic equilibrium, but only on the run of temperature and electron density with optical depth in *K*.

A *cool* absorbing layer above a *hot* emitting layer, as suggested by Engvold (1966) and Teplitskaja and Firstova (1976) is not necessary to produce an absorption feature in the line centre of *H* and *K*.

It could be argued that the disagreement between the prediction of central absorption features of the optically thick models *A*, *B*, and *C* and the absence of this absorption in most observations is a major objection to the optically thick models. But we do not believe that such a conclusion necessarily follows. We cannot rule out the possibility that the umbral chromosphere *is* optically thick in the K line, and that the self-reversal predicted by our plane-parallel static model is obliterated by the effects of time- and space-dependent dynamical processes on the line profile. The important role of such processes in the formation of the quiet sun K line profile has been discussed by Durrant et al. (1976) and others, and occurrence of dynamical phenomena in umbra chromospheres is well documented (Beckers and Schultz, 1972; Giovanelli, 1972).

We would like to include such effects in our models. Unfortunately, long exposure times and problems with false light prevent the spectroscopic study of non-flashing sunspot fine structure, and there are presently no theories for umbral dynamics which are developed to the point of predicting the parameters we need for a line formation study. In the absence of both theoretical and observational guidelines we cannot construct a detailed dynamical model and then compute a spatially averaged profile for comparison with the observations. To illustrate what could occur, however, we have convolved the theoretical profiles with a Gaussian macro-turbulence profile of 5 km s^{-1} amplitude. As can be seen from

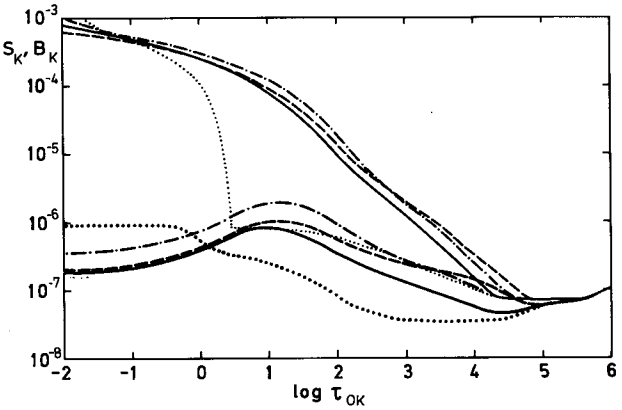

Fig. 6. Line centre source function of K line (heavily drawn) and Planck function (weakly drawn) versus optical depth of K line centre for model *A* (full line), *B* (dashed), *C* (dash-dotted), and *D* (dotted). Thick atmospheres (*A*–*C*) have the source function maximum at $\tau_{0K} > 1$, thin atmospheres (*D*) at $\tau_{0K} < 1$

Figure 4, this completely removes the self-reversal in the optically thick models. There is no physical basis for the amplitude or even the form of the macro-turbulence and, consequently, there is little point in comparing the smeared profiles with the observations. However, this velocity model illustrates the possibility that dynamical processes in optically thick umbral chromospheres could lead to unreversed profiles. We might mention that theoretical non-LTE emission line profiles almost always exhibit central absorption features deeper than those of the corresponding observations (e.g. quiet sun K line; Ayres, 1975; plage K line; Shine and Linsky, 1974). In these cases too, dynamical processes could be responsible for the disparity.

When comparing the optically thick models differentially we notice two effects. First, in going from model *A* to model *B*, the overall increase in emerging intensities is small. But the ratio I_{K3}/I_{H3} of the Gaussian convolved profiles, which is now a measure of the ratio of the *total* emission in H and K, decreases from 1.38 to 1.24. This is due to the deeper onset of the chromospheric temperature rise in model *B*. Second, in going from model *A* to model *C*, we see large increases in the emergent core intensities because of the overall increase of temperature and electron density. The λ8542 line exhibits a trace of line centre emission in model *C*.

4.2. *Micro-Velocities and Radiation Temperatures*

We investigate first the influence of the run of the micro-velocity on the K line profile and then the effect of varying the radiation temperatures in the Balmer continuum and in the ionizing continua of Ca II, which cause some uncertainties in both the atmospheric models and the Ca II ionization equilibrium. For these test calculations we use the thick atmospheric model *A* of Figures 2 and 3, a three-level plus continuum model atom for Ca II, and treat the radiative transfer with CRD. The computational simplifications do not invalidate the conclusions drawn from differential trends.

Figure 7 gives several curves for the micro-velocities. (Curve 4 was designed for the thin model.) As already mentioned, a micro-velocity of $v_t = 1$ km s^{-1} seems to be an upper limit at large depths (Kjeldseth Moe, 1973). Above sunspots, at levels of the transition zone to the corona, Cheng et al. (1976) observe an *increase* with height (temperature) of the non-thermal broadening. Their measured value of 9 km s^{-1} at the 16 000 K level is also included in Figure 7. A *decrease* of the Doppler broadening with height, as suggested by Teplitskaja and Efendieva (1975), does not fit easily to the above boundary values. Therefore we have not included such a run of micro-velocities in our calculations. Figure 8*a* shows the resulting profiles of the K line. The bigger the micro-velocity the broader is the line profile and the less pronounced is the self-reversal. We cannot, however, force the self-reversal to disappear for reasonable values of the micro-turbulence.

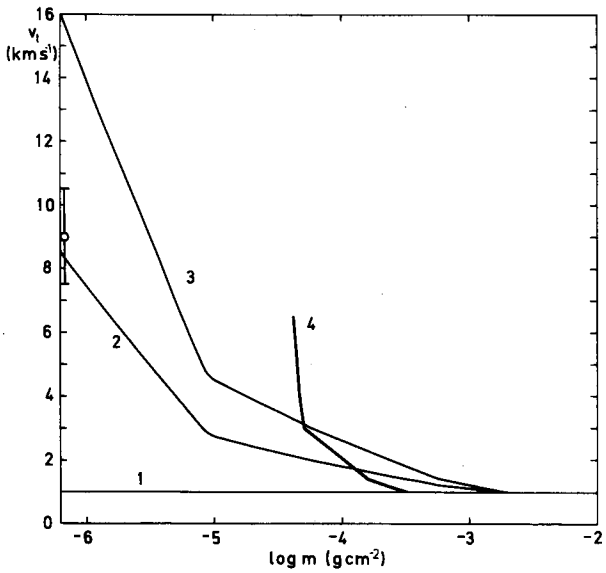

Fig. 7. Several runs of micro-turbulence. Curve 4 is used only for the thin model *D*. Φ: non-thermal broadening at the 16 000 K level measured by Cheng et al. (1976)

Figure 8*b* shows the differential effects on the K line of different ionizing radiation temperatures. If we assume that the Balmer continuum radiation temperature is only 3000 K instead of the reference value 3500 K the hydrogen ionization in the chromosphere is reduced. As a result of the smaller electron density the source function and the emergent intensity of the K line is weakened (profile 2 in Fig. 8*b*). On the other hand, if we assume a higher temperature than the usual $T_R < 4000$ K for the ionization continua of Ca II (this could be produced, for example, if there were many strong emission lines below 1500 Å) the ionization equilibrium is shifted in favour of Ca III. This reduces the optical thickness of the high temperature chromosphere and weakens the emission of the K line (Fig. 8*b*, profile 3).

4.3. *A Model*

One of the aims of this study is to use the Ca II spectrum to provide a reference model for the chromosphere above sunspots. We are inclined to reject a thin model: it appears to be easier to account for the failure of most observations to reveal the self-reversal predicted by the thick model than to account for the line intensity ratio predicted by a thin model. We propose as reference model the thick model *C* of Figures 2 and 3, together with the run of micro-turbulence of curve 2 in Figure 7. The emergent line profiles are shown in Figure 9. The theoretical K line closely resembles the profiles observed by Engvold (1967). After smoothing of the self-reversed

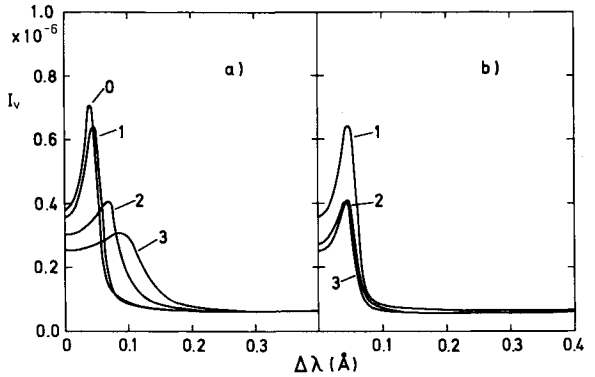

Fig. 8a. Effect of different micro-velocities on the K line emission core in model A, $\cos\theta = 0.89$. Label 0: $v_t = 0$ km s^{-1}; labels 1–3; curves 1–3 of Figure 7. **b** Effect of different radiation temperatures in the ionization continua. Label 1: $T_{R,B} = 3500$ K; $T_{R,4S\text{-cont}} =$. 3900 K; $T_{R,4P\text{-cont.}} = 3400$ K;
Label 2: $T_{R,B} = 3000$ K; others the same as for 1
Label 3: $T_{R,B} = 3500$ K; $T_{R,4S} = T_{R,3D} = T_{R,4P} = 5500$ K.
Profiles in (a) and (b) from a three-level plus continuum model atom and with complete redistribution

emission cores of the H and K lines by a Gaussian distributed macro-velocity with 5 km s^{-1} amplitude the profiles exhibit closely the features reported by the other investigators as listed in Table 1. The ratio $I_{K3}/I_{H3} \approx 1.18$ lies well in the observed range. The K_1 position is mainly a function of the non-thermal velocities. The wing beyond K_1 is extremely flat. The IR lines also fulfill the requirements of Table 1.

We compare our reference model with the quiet chromosphere model of Vernazza et al. (1973) and the umbra model of Baranovski (1974) in Figure 10. We have tried the latter model and have found that with the abundance of Ca used here the K line emission is too strong by factors five to ten. The temperature and electron density seem to be too high in the upper layers of Baranovski's model.

At the 16 000 K level, our model possesses a pressure of 0.03 dyn cm^{-2}, which is five times smaller than the coronal pressure above the quiet chromosphere, and an electron density of 6×10^9 cm^{-3}, which is four times lower than the value estimated by Cheng et al. (1976) for the 36 000 K level above umbrae. The temperature gradient in the top layers is about 8 K km^{-1}.

5. Conclusion

We have presented a model of the chromosphere above sunspots which can explain many aspects of the observed emission features in the Ca II, H and K lines and the IR lines of Ca II. To explain the line centre intensity ratio of K and H, which is close to unity, we have chosen an optically thick chromosphere. Such a model exhibits self-reversals in H and K line cores which are rarely observed (Engvold, 1967).

We can suggest several possible explanations of this problem. First, we should wait for a treatment of the non-LTE radiative transfer problem in the presence of magnetic fields. The emission features of H and K are expected to be broadened by the Zeeman-splitting. Second, spectrograms of the best available resolution in wavelength, space and time should reveal if the H and K lines exhibit self-reversed profiles characteristic of an optically thick atmosphere on very small scales. Third, macroscopic velocities such as those observed by Giovanelli (1972) could change the asymmetric doubly peaked profiles predicted by thick models into asymmetric single emission peaks as a result of differential velocity fields, just as in the quiet chromosphere. (See e.g. Durrant et al., 1976.) This effect should be studied both observationally and theoretically. Finally, we do not claim uniqueness for our umbra model. Possibly, there exists a *static* model which gives pure emission cores with the correct intensities (and intensity ratios). However, this would probably be a very special model and unlikely to be realized in all the different kinds of umbrae. We feel that a search for such a model is unwarranted, in view of the many observational uncertainties and of the other possible explanations.

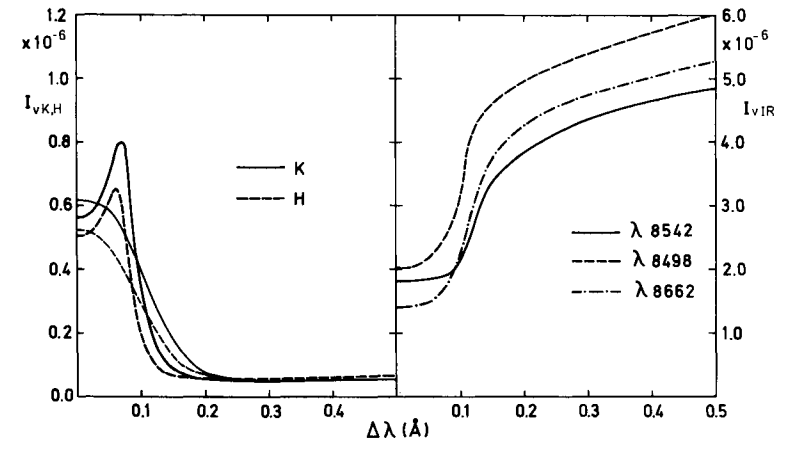

Fig. 9. Profiles of the Ca II lines emitted from the suggested umbra chromosphere model, $\cos\theta = 0.89$. H and K are again convolved with a Gaussian profile with an amplitude of 5 km s^{-1} (weak lines)

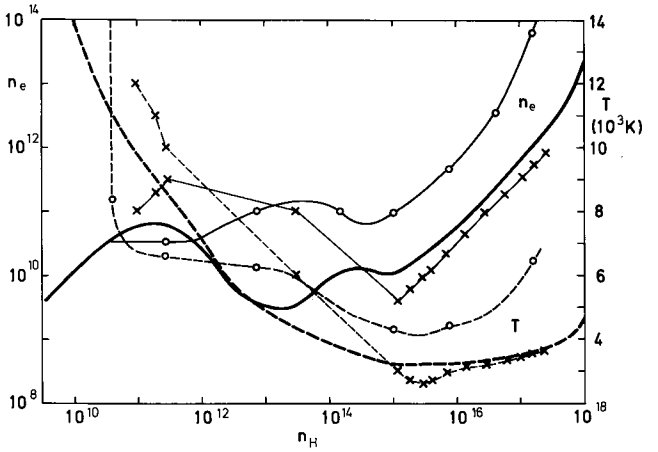

Fig. 10. Electron number density (full lines) and temperature (dashed lines) versus hydrogen number density. Heavy lines: suggested umbra model; crosses: umbra model of Baranovski (1974); open circles: *photospheric* model of Vernazza et al. (1973)

We consider the umbra model presented above as a starting point for further investigations. It should be checked and improved with additional observations, including lines and continua in the far ultra-violet spectral region. We have already mentioned the pressing need for high quality observations of the Ca II infra-red triplet. The model is also intended as a guide for magneto-dynamic considerations which treat the energy balance in umbral chromospheres. Our model may help answer the question of the distribution of energy dissipation in sunspots.

Appendix

A.1. The Ionization of Hydrogen

We have to clarify the meanings of ε_0 and G in Equation (5):

$$\varepsilon_0 = \frac{C_{1K}}{R_{K1}}\left[1 + \frac{C_{12}(1 + C_{2K}/R_{K2})/(R_{2K}/R_{K2})}{C_{1K}(1 + C_{2K}/R_{2K} + C_{21}/R_{2K})}\right], \quad \text{(A.1)}$$

$$G = \frac{1 + (C_{12}/C_{1K})(R_{2K} + C_{2K})/(R_{2K} + C_{2K} + C_{21})}{1 + (C_{12}/C_{1K})(R_{K2} + C_{2K})/(R_{2K} + C_{2K} + C_{21})}. \quad \text{(A.2)}$$

Linsky (1968) gives slightly different formulae. However, a close inspection of the steady state rate equations (Mihalas 1970) and of the procedure of Dietz and House (1965) convinces us that the expressions (A.1) and (A.2) are appropriate. The C_{ij}'s represent collisional rate coefficients proportional to the electron density with

$$C_{ij} = n_e\Omega_{ji}(T)\exp(-h\nu_{ij}/kT), \quad (j > i) \quad \text{(A.3)}$$

and

$$C_{ji} = n_e\Omega_{ji}(T)g_i/g_j \quad \text{(A.4)}$$

where the g's are the statistical weights. For Ω_{ji} we choose values independent of temperature from a table by Avrett (1974)

$$\Omega_{21} = 2.5 \times 10^{-8}$$

$$\Omega_{K1} = 3.0 \times 10^{-9}$$

$$\Omega_{K2} = 1.0 \times 10^{-7}.$$

For the radiative rate coefficients we neglect stimulated emission and have the formulae

$$R_{Ki} = 4\pi\int_{\nu_{iK}}^{\infty}\frac{\alpha_i(\nu)}{h\nu}\frac{2h\nu^3}{c^2}\exp(-h\nu/kT)d\nu, \quad (i = 1, 2) \quad \text{(A.5)}$$

and

$$R_{2K} = 4\pi w\int_{\nu_{2K}}^{\infty}\frac{\alpha_2(\nu)}{h\nu}B_\nu(T_{R,B})d\nu, \quad \text{(A.6)}$$

where $B_\nu(T_{R,B})$ is the Planck function at the radiation temperature of the Balmer continuum $T_{R,B}$ and w is the dilution factor. For the frequency dependence of the absorption cross-sections we take

$$\alpha_i(\nu) = \alpha_{i0}\left(\frac{\nu_{iK}}{\nu}\right)^3, \quad (i = 1, 2) \quad \text{(A.7)}$$

and from Allen (1973) at the head of the continua ($\nu = \nu_{iK}$) we have

$$\alpha_{i0} \approx 7.9 \times 10^{-18} \times i. \quad \text{(A.8)}$$

In Equation (A.8) we set the Gaunt factors equal to unity.

A.2. Atomic Data of Ca II

The data given below are mostly interpolations and simplifications of the set of atomic data compiled by Shine and Linsky (1974). We feel that such simplifications are justified in view of the preliminary nature of our model calculations and of the many observational uncertainties.

Table A.1 summarizes the data used. The abundance of Ca is taken from Shine et al. (1975). The ionization frequencies and statistical weights of the levels as well as the wavelengths, oscillator strengths (or continuous absorption coefficients) for radiative transitions are given. The definition of the α_{i0}'s is the same as in Equation (A.7). For the collisional rate coefficients we use the expression (A.3) with a temperature dependence according to

$$\Omega_{Ki}(T) = CE_{Ki} \times \sqrt{T} \quad \text{(A.9)}$$

for the ionizing collisions and

$$\Omega_{ji}(T) = CE_{ji}/\sqrt{T}, \quad (j > i) \quad \text{(A.10)}$$

for the bound-bound collisions. Values of CE_{ji} are given in Table A.1. Collisions by neutral hydrogen atoms are neglected.

Table A.1

Abundance 2.14×10^{-6}						
Level Parameters						
Level	1	2	3	4	5	6 (cont.)
Term Designation	$4s^2S_{1/2}$	$3d^2D_{3/2}$	$3d^2D_{5/2}$	$4p^2P_{1/2}$	$4p^2P_{3/2}$	$4s^2p^6{}^1S_0$
Ionization Frequency (10^{15} Hz)	2.87158	2.46211	2.46029	2.11601	2.10933	0.0
g	2	4	6	2	4	1
Radiative Transitions						
Transition	5–1	5–2	5–3	4–1	4–2	
λ (Å)	3934	8498	8542	3968	8662	
f	0.66	0.00883	0.053	0.33	0.0442	
Transition	6–1	6–2	6–3	6–4	6–5	
λ (Å)	1044	1218	1219	1417	1422	
α_{i0} (10^{-18} cm^2)	0.22	6.2	6.2	2.4	2.4	
Collisional Transitions						
Transition	5–1	5–2	5–3	5–4	4–1	
CE	4.1 (−5)	2.1 (−5)	6.5 (−5)	4.3 (−5)	2.1 (−5)	
Transition	4–2	4–3	3–1	3–2	2–1	
CE	4.9 (−5)	0.44 (−5)	3.6 (−5)	4.6 (−5)	2.4 (−5)	
Transition	6–1	6–2	6–3	6–4	6–5	
CE	1.45 (−10)	1.88 (−10)	1.88 (−10)	2.68 (−10)	2.68 (−10)	

The damping constant of the Voigt profile, Equation (6), is represented by

$$a = (\Gamma_R + \Gamma_{VW} n_H)/4\pi\Delta\nu_D \qquad (A.11)$$

where n_H is the number density of neutral hydrogen and $\Delta\nu_D$ the Doppler width. For all lines we use a radiative damping width of

$$\Gamma_R = 1.5 \times 10^8 \text{ s}^{-1}$$

and a Van der Waals broadening constant of

$$\Gamma_{VW} = 1.6 \times 10^{-8} \text{ cm}^3 \text{ s}^{-1}.$$

Acknowledgements. We wish to express our deepest gratitude to Drs. L. H. Auer and J. N. Heasley for their invaluable support with the difficult calculations. It is a pleasure to thank Dr. L. E. Cram for discussions and helpful comments during the preparation of the manuscript. The calculations were carried out on the UNIVAC 1106 computer of the Rechenzentrum der Universität Freiburg.

References

Allen, C. W.: 1973, Astrophysical Quantities, 3rd edition, Athlone Press, p. 96
Athay, R. G., Skumanich, A.: 1968, *Solar Phys.* **3**, 181
Auer, L. H., Heasley, J. N.: 1976, *Astrophys. J.* **205**, 165
Auer, L. H., Heasley, J. N., House, L. L.: 1977, *Astrophys. J.* **216**, 531
Auer, L. H., Heasley, J. N., Milkey, R. W.: 1972, Kitt Peak National Observatory Contribution No. 555
Avrett, E. H.: 1974, private communication
Ayres, T. R.: 1975, Ph.D. thesis, University of Colorado
Baranovski, E. A.: 1974, *Izv. Krymsk. Astrofiz. Obs.* **51**, 56
Beckers, J. M.: 1976, *Astrophys. J.* **203**, 739
Beckers, J. M., Schultz, R. B.: 1972, *Solar Phys.* **27**, 61
Beckers, J. M., Tallant, P. E.: 1969, *Solar Phys.* **7**, 351
Biermann, L.: 1941, *Vierteljahresschr. Astron. Gesellsch.* **76**, 194
Burgess, A.: 1965, *Smithsonian Special Report* **174**, 47
Cheng, C.-C., Doschek, G. A., Feldman, A.: 1976, *Astrophys. J.* **210**, 836
Danielson, R. E., Savage, B. D.: 1968, *IAU Symp.* **35**, (Kiepenheuer ed.), 112
Dietz, R. D., House, L. L.: 1965, *Astrophys. J.* **141**, 1393
Durrant, C. J., Grossmann-Doerth, U., Kneer, F.: 1976, *Astron. Astrophys.* **51**, 95

Engvold, O.: 1966, *Astrophysica Norvegica* **10**, 101
Engvold, O.: 1967, *Solar Phys.* **2**, 234
Foukal, P. V., Huber, M. C. E., Noyes, R. W., Reeves, E. M., Schmahl, E. J., Timothy, J. G., Vernazza, J. E., Withbroe, G. L.: 1974, *Astrophys. J. Letters* **193**, L143
Gingerich, O., Noyes, R. W., Kalkofen, W., Cunny, Y.: 1971, *Solar Phys.* **18**, 347
Giovanelli, R. G.: 1972, *Solar Phys.* **27**, 71
Heasley, J. N., Kneer, F.: 1976, *Astrophys. J.* **203**, 660
Hénoux, J. C.: 1969, *Astron. Astrophys.* **2**, 288
House, L. L., Steinitz, R.: 1975, *Astrophys. J.* **195**, 235
Jefferies, J. T., White, R. O.: 1960, *Astrophys. J.* **132**, 767
Kjeldseth Moe, O.: 1973, *Solar Phys.* **33**, 393
Kneer, F.: 1972, *Astron. Astrophys.* **18**, 39
Kneer, F.: 1975, *Astrophys. J.* **200**, 367
Labs, D., Neckel, H.: 1968, *Z. Astrophys.* **69**, 1
Linsky, J. L.: 1968, *Smithsonian Special Report.* **274**
Linsky, J. L.: 1970, *Solar Phys.* **11**, 355
Linsky, J. L., Avrett, E. H.: 1970, *Publ. Astron. Soc. Pacific* **82**, 169
Marik, M.: 1967, *Soviet Astron.—AJ* **11**, 264
Mattig, W., Kneer, F.: 1977, *Astron. Astrophys.*
Mihalas, D.: 1970, *Stellar Atmospheres*, Freeman, San Francisco, p. 144
Mustel, E. R., Tsap, T. T.: 1960, *Izv. Krymsk. Astrofiz. Obs.* **22**, 75
Omont, A., Smith, E. W., Cooper, J.: 1973, *Astrophys. J.* **182**, 283
Parker, E. N.: 1974, *Solar Phys.* **36**, 249
Shine, R. A., Linsky, J. L.: 1972, *Solar Phys.* **25**, 357
Shine, R. A., Linsky, J. L.: 1974, *Solar Phys.* **39**, 49
Shine, R. A., Milkey, R. W., Mihalas, D.: 1975, *Astrophys. J.* **199**, 724
Stellmacher, G., Wiehr, E.: 1970, *Astron. Astrophys.* **7**, 432
Teplitskaja, R. B., Efendieva, S. A.: 1971, *Soln. Dannye* **3**, 80
Teplitskaja, R. B., Efendieva, S. A.: 1973, *Solar Phys.* **28**, 369
Teplitskaja, R. B., Efendieva, S. A.: 1975, *Solar Phys.* **43**, 293
Teplitskaja, R. B., Firstova, N. M.: 1976, *Solar Phys.* **48**, 103
Vernazza, J. E., Avrett, E. H., Loeser, R.: 1973, *Astrophys. J.* **184**, 605
White, R. O., Suemoto, Z.: 1968, *Solar Phys.* **3**, 523
Zwaan, C.: 1965, *Rech. Astron. d'Utrecht* **17**, part 4

Astron. Astrophys. 65, 17–28 (1978)

ASTRONOMY AND ASTROPHYSICS

The Chromosphere above Sunspot Umbrae.
II. The Interpretation of the H, K, and IR Lines of Ca II*

F. Kneer and W. Mattig

Fraunhofer-Institut, Schöneckstr. 6, D-7800 Freiburg, Federal Republic of Germany

Received July 15, 1977

Summary. The chromospheres above sunspot umbrae are investigated by comparing calculated and observed profiles of the Ca II H, K, and infra-red lines. Statistical steady state is assumed for the level populations. We test several model chromospheres in hydrostatic equilibrium. We distinguish between chromospheres which are optically thick and optically thin at the centre of the K line. In view of the observed intensity ratio $I_{K3}/I_{H3} \approx 1.15$ we are forced to adopt a thick model as reference chromosphere.

Key words: chromosphere — sunspot umbra — Ca II lines

1. Introduction

The spectra of sunspot umbrae show emission cores in the Ca II H and K lines. This indicates that the radial temperature profile above a sunspot passes through a minimum: in other words, that umbrae possess chromospheres (Linsky and Avrett, 1970).

With regard to the energy balance of sunspots Biermann (1941) suggested that the convective energy transport is largely *prohibited* by the magnetic field and that therefore sunspots are cooler than the normal photosphere. Danielson and Savage (1968) discussed whether the missing flux in sunspots could be carried by magneto-acoustic waves. In contrast to the Biermann picture, Parker (1974) proposed that sunspots are regions of *enhanced* energy transport in the form of Alfvénic flux so that as a net effect the umbral material is cooled. A study of the structure and dynamics of the atmosphere above sunspots should help choose between these two very different points of view (Beckers, 1976; Foukal et al., 1974).

The question of energy balance in sunspots is interesting in its own right, but in addition we can learn a great deal by comparing and contrasting the chromospheres of sunspots with the chromosphere of the quiet sun. Since we know that the magnetic pressure in sunspots is comparable to—or larger than—the gas pressure we expect the magnetic field to influence the energy transport and dissipation mechanisms (Marik, 1967) and to produce chromospheres very distinct from the ones of the quiet regions without magnetic fields. Thus, we can think of the two types of atmospheres, umbral and quiet chromospheres, as two nearby stellar laboratories with different —only partly understood—equipment.

On these grounds it is important to know the structure of both types of chromospheres. However, while an enormous number of investigations of the quiet chromosphere and its fine structure have been undertaken, very little work has been devoted to the umbral chromosphere. The reason for the underrepresentation of research in this field is obvious: both observational and interpretational difficulties far surpass the problems met in studies of the quiet chromosphere. Observationally, the high intensity radiation from the ambient area on the sun falsifies the true umbral radiation through atmospheric and instrumental scattering of light and through seeing effects. In the far ultra-violet region the spot emission seems to be comparable to the emission from the surrounding medium so that false light plays a minor role (Foukal et al., 1974; Cheng et al., 1976). However, observations in this spectral region with high spatial and wavelength resolution have become available only in the last few years. Interpretationally, our ability to treat non-LTE line formation in magnetic fields has only recently improved (Omont et al., 1973; House and Steinitz, 1975; Auer et al., 1977).

Despite these difficulties we feel that it is possible to use existing observations to draw some conclusions on the structure of umbral chromospheres, at least as a starting approximation. We use here as diagnostic probes only the five strongest lines of Ca II. The next section is devoted to the observational data of these lines. Section 3 deals with the assumptions and numerical methods concerning the treatment of both the model atmosphere and the Ca

* Mitteilungen aus dem Fraunhofer-Institut No. 150

atom. In Section 4 we discuss several models and compare them with results of other investigators.

2. Observations

We do not present new observations here, but rather collect some prominent observational features of the Ca II H, K and IR lines. It is important to notice here that we are not able to give exact figures of calibrated observations for two reasons. First, sunspot structure differs from one spot to another and sunspots exhibit a variety of different profiles of the same line. Second, as already mentioned, the observed spot intensities are falsified by scattered light whose influence may be seen from the following formula (Zwaan, 1965)

$$I' = (1 - \beta)I + \beta I^a. \quad (1)$$

Here, I and I' are the true and observed spot intensities, respectively, βI is the fraction of light scattered *out* of the beam and βI^a is the fraction of light scattered *into* the beam from the ambient area. We see at once from Equation (1) that for equal intensities in spot and surrounding area ($I = I^a$) the scattering has no influence. On the other hand, it follows for (relatively) small sunspot intensities ($I \ll I^a$) that the observed intensities are strongly falsified. Usually (Kneer, 1972), the continuum intensity ratio of sunspot to photosphere *decreases* towards shorter wavelengths (in the visible spectral range), while the fraction of scattered light *increases*. As a consequence, at a continuum wavelength near the H and K lines, the false light may override the weak intensity from the spot. From this discussion we learn to accept observed sunspot line profiles with caution.

With the above in mind we summarize the relevant properties of the H, K, and IR lines in sunspots in Table 1. The first column of Table 1 indicates the spectral feature, the second column its behaviour, and the third column the sources. Most of the figures refer to observations close to the disc centre. We exclude such prominent observational facts as brightness and velocity oscillations (Beckers and Tallant, 1969; Beckers and Schultz, 1972) and line asymmetries (Teplitskaja and Firstova, 1976). We concentrate in this paper on the interpretation in terms of time independence: the modification of the

Table 1

H and K lines:		
I_{K3}	$0.5 \cdots 1.0 \times I^{\odot}_{K3}$*	M, E, L, SL
	$\approx 0.5 \cdots 1.0 \times 10^{-6}$ erg cm^{-2} s^{-1} sterad^{-1} Hz^{-1}	
self-reversal?	yes ($I_{K2} \approx I_{K3}$, self-reversal small,	E, TEa (near limb)
	$\Delta\lambda_{K2} \approx 0.06$ Å	E
	no	MK, L, SL, MT
I_{K1}	$0.1 \cdots 0.3 \times I_{K3}$	MK, L, E, SL, MT
$\Delta\lambda_{K1}$	0.25 ··· 0.35 Å	MK, L, E, SL, MT
FWHM**	0.2 ··· 0.25 Å	MK, TEb
wings beyond K_1	flat compared to wings in plages	MT
I_{K3}/I_{H3}	1.0 ··· 1.3	MK, L, TF
	1.7	SL
I_{K1}/I_{H1}	$\lesssim 1.0$	MK, L, SL
IR lines:		
emission cores?	no! pure absorption lines	
residual intensities at line centre	~0.25	
relative intensities at line centre	$I_{8498} > I_{8542} > I_{8662}$	SL
relative intensities in wings	$I_{8498} > I_{8662} > I_{8542}$	

Sources: E: Engvold (1967); L: Linsky (1970); MK: Mattig and Kneer (1977); MT: Mustel and Tsap (1960); SL: Shine and Linsky (1972); TEa: Teplitskaja and Efendieva (1971); TEb: Teplitskaja and Efendieva (1973); TF: Teplitskaja and Firstova (1976)

* $I^{\odot}_{K3}$ is the intensity measured from the quiet chromosphere

** FWHM = full width at intensities $(I_{K3} + K_{K1})/2$. K_1 is the minimum in the line profile

resulting models by a dynamic interpretation will be an important future step.

Let us comment briefly on some items of Table 1: The intensity of the centre of the K line, I_{K3}, is only weakly contaminated by scattered light because it differs only little from the intensity of the quiet chromosphere, $I^{\odot}_{K3}$. We can estimate the latter by comparing the measurements of White and Suemoto (1968) with the continuum intensity at 4000 Å calculated from the Harvard Smithsonian Reference Atmosphere (Gingerich et al., 1971), which is in good agreement with the calibrated observations of Labs and Neckel (1968). From this one is led to $I^{\odot}_{K3} \approx 1.0 \times 10^{-6}$ erg cm^{-2} s^{-1} sterad^{-1} Hz^{-1} at disc centre. Linsky (1970) and Shine and Linsky (1972) present their line profiles with respect to the local continuum in the umbra. If we admit that, due to false light, their continuum intensities at the K line are too high by possibly 10 to 50 percent we may conclude from their data that the continuum and line centre intensity are approximately equal in the spot. Reasonable umbra models of the continuum emitting layers (see Section 4) give values of $I_{\rm cont} \approx 6.0 \times 10^{-7}$ erg cm^{-2} sterad^{-1} = $0.6 I^{\odot}_{K3}$. This is in line with the results of other observers. (See Linsky and Avrett, 1970, for a similar estimate of the K_3 intensity in sunspots.)

We defer comments on the question of the self-reversal to the discussion of our models (Section 4). The intensity of K_1 (H_1) and also the wing intensities beyond K_1 may be affected by false light and most of the published values are probably too high by some 10 to 50 percent. However, the flat damping wings of the K line, as shown to a distance of about 3.5 Å from line centre in the observations of Mustel and Tsap (1960), are worth noticing. The intensity ratio I_{K3}/I_{H3} will turn to an important diagnostic tool for the investigation of the thickness of the umbral chromosphere and will also be discussed in Section 4. The position of the K_1 minimum in sunspots is reported consistently by many observers. Possibly, it is only little influenced by scattered light.

The only observations of the IR lines available to us are those of Shine and Linsky (1972). Unfortunately, as they themselves state, their data contain contributions from the surrounding penumbra and plage regions because of poor seeing conditions. We take for granted that we are dealing with pure absorption profiles. Unless contradictory observations turn up this is an additional observational constraint for modelling chromospheres above sunspots. Clearly, there is a pressing need for more observations of these lines.

3. Assumptions and Methods

In this section we outline the several assumptions and methods used here for the modelling of chromospheres and for the calculation of both the ionization equilibrium of the calcium atom and the emergent line profiles.

3.1. Hydrostatic Equilibrium

For each model atmosphere we specify a one-dimensional run of temperature $T(p_{\rm tot})$ as a function of total pressure $p_{\rm tot}$ or, equivalently, of column mass density m by means of the equation for hydrostatic equilibrium

$$p_{\rm tot} = gm \tag{2}$$

where g is the surface gravity acceleration. At the upper boundary, for $m = 0$, we have put $p_{\rm tot} = 0$. The column mass density is related to the mass density ρ and geometric height h through

$$dm = -\rho dh. \tag{3}$$

For many needs one is forced to calculate the mass density ρ as a function of the temperature and the electron density n_e. The latter is an implicit function of abundances, temperature, gas pressure p_g, and radiation fields J_ν at all frequencies ν, which influence the ionization equilibrium within the gas:

$$F(n_e, \varepsilon_i, T, p_g, J_\nu) = 0. \tag{4}$$

We use the same chemical composition as in the Kitt Peak code (subroutine STATE) of Auer et al. (1972), including calcium as an additional electron donor at low temperatures. This code treats the formation of the H_2 and H_2^+ molecules and the ionization of the metals, He, and H^- in LTE. The non-LTE ionization of hydrogen is discussed below. With a known functional or numerical dependence of the ionization equilibria on n_e, T, and p_g we solve Equation (4) iteratively for n_e by a secant method.

3.2. The Ionization of Hydrogen

For the non-LTE deviation factor b_1 of the hydrogen ground level we adopt an analytic approximation due to Kalkofen (quoted by Linsky, 1968)

$$1/b_1(\tau_0) \approx G[1 + (\sqrt{\varepsilon_0} - 1) \exp(-\sqrt{3\varepsilon_0}\tau_0)], \tag{5}$$

where τ_0 is the optical depth at the head of the Lyman continuum. The above formula is an extension from a treatment by Dietz and House (1965) of a ground level plus continuum hydrogen atom to an inclusion of the second bound level with Ly-α in detailed radiative balance. Thus, ε_0 is essentially the ratio of collisional to radiative recombination to the ground level and G is a correction factor which accounts for radiation and collision processes to the second bound level. (The reader is referred to the Appendix for the detailed expressions of ε_0 and G.) The factor $\sqrt{3}$ in the exponent is a consequence of the Eddington approximation.

Except for the mean radiation field in the Balmer continuum only local quantities (n_e, T, τ_0) enter into the right-hand side of Equation (5). The intensity of the

Balmer continuum may be specified by a radiation temperature $T_{R,B}$ by the choice of a special column mass density m_0 in such a way that

$$T_{R,B}(m) = T(m) \quad \text{for } m > m_0,$$

and

$$T_{R,B}(m) = T(m_0) \quad \text{for } m < m_0.$$

The choice of m_0 is difficult because no calibrated observations of the Balmer continuum in sunspots are available. One preliminary choice of m_0 could be the point in the atmosphere where the head of the Balmer continuum has an optical depth of about unity. We believe that this point lies deeper in the atmosphere than the temperature minimum. We usually choose m_0 at $T = 3500$ K; we discuss the influence of $T_{R,B}$ in the next section. With the specification of $T_{R,B}$ it is possible to treat the hydrogen ionization as an initial value problem with $\tau_0 = 0$ at the top of the atmosphere.

The main assumption underlying the approximate formula (5) is that none of the parameters vary with height; this is equivalent to the assumption of an isothermal atmosphere with constant density and constant $T_{R,B}$. Certainly, real atmospheres need a more detailed treatment of the radiation fields, but we wish to defer a more consistent calculation of the hydrogen ionization to a future investigation when, hopefully, observational data of the Ly-α line, the Ly-continuum, and the Balmer continuum in sunspots will be available. We apply the above formula because it provides a better approximation than LTE for the contribution of hydrogen to the electron density where deviations from LTE are important. According to our experience, Equation (5) leads to electron densities in quiet chromospheric models with an accuracy of 50 percent or better compared with self-consistent non-LTE calculations.

3.3. *The Ionization of Calcium*

(a) The Ca II/Ca I Density Ratio

A self-consistent determination of the ratio of the Ca II to Ca I densities has to account for many collisional and radiative transitions (Linsky, 1968). We avoid this difficult task by assuming that Ca I is ionized in LTE. For this purpose we adopt from Linsky (1968) an ionization energy for Ca I of $\chi_I = 6.11$ eV and a ratio of the partition functions at low temperatures of $U_{II}/U_I = 2$. Table 2 gives the density ratio if Ca II to Ca I for some heights near the temperature minimum in one of our models. We see that even near the temperature minimum the Ca I density is less than 25 percent of the total Ca density. We may argue as follows that this is probably an overestimate: Below a temperature of 4000 K dielectronic recombinations do not seem to play the dominant role in populating the Ca I atom (Burgess, 1965), so that photoionizations and -recombinations are probably the important processes determining the Ca II/Ca I density ratio. Then, since the ionizing radiation fields at the temperature minimum usually originate in deeper layers corresponding to a higher radiation temperature, the levels of the lower ionization stage tend to be depopulated at a higher rate than under LTE conditions. (See for instance the behaviour of the ground level deviation factor of hydrogen at the *photospheric* temperature minimum in the model of Vernazza et al., 1973.) We thus conclude that a more detailed treatment of the Ca II/Ca I density ratio would have little influence upon our conclusions regarding the line profiles of Ca II.

Table 2

m (g cm^{-2})	T (K)	$n_{\mathrm{Ca\,II}}/n_{\mathrm{Ca\,I}}$
0.01	3350	102
0.0315	3200	26
0.1	3200	12
0.315	3250	6.7
1.0	3390	5.7
2.14	3480	5.0
4.57	3600	4.8
10	3820	6.2

(b) The Ca II–Ca III Level Populations

We next consider our model representation of the Ca II ion of Figure 1. Only the five lowest levels plus the continuum (Ca III) are included. For test calculations we will restrict the model ion further, to levels 1, 3, 5, and 6; this is a fair representation according to Linsky (1968) and to our experience with low temperature atmospheres. The atomic data used in this investigation are given in the Appendix.

It is our aim in this investigation to study the line profiles of the five strongest Ca II lines emerging from model atmospheres. For this purpose we assume a statistical steady state for the level populations. The steady state equations and the radiative transfer equations in *one*-dimensional geometry are simultaneously solved with the complete linearization method in the form worked out by Auer and Heasley (1976). In this scheme the first-order corrections to the *radiative rates* are computed, and this is superior to calculating corrections to the *radiation fields* when many broad lines are to be treated. The influence of the magnetic field is excluded and deferred to a forthcoming investigation.

We treat only *line* transitions in detail. The photoionization rate coefficients are kept fixed for each model atmosphere by specifying a radiation temperature similar to the Balmer radiation temperature in the hydrogen

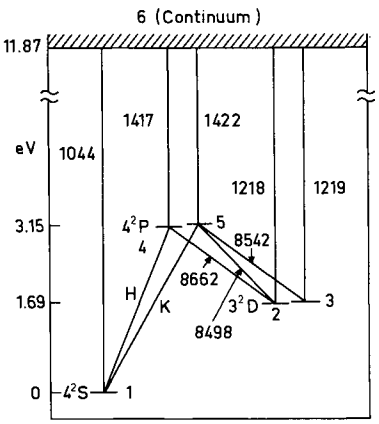

Fig. 1. Energy level diagram of Ca II and radiative transitions

ionization problem. Such a procedure causes uncertainties in our calculations of the level populations because of the lack of observations of the ionization continua of Ca II below 1422 Å in sunspots. However, some guidance can be obtained by the height of formation of the background continua, essentially the C I continua at 1444 Å, 1239 Å, and 1100 Å, in the quiet chromosphere. According to Vernazza et al. (1973), these are formed between 750 km and 1200 km, at pressures of roughly 8 to 200 dyn cm^{-2}. Assuming that carbon is mainly neutral in this layer in both sunspot and quiet chromosphere we obtain with Equation (1) column mass densities of about 3×10^{-4} to 7×10^{-3} g cm^{-2} as bounds to the region where the background continua are becoming optically thick. As standard values we choose the points $m_0 = 10^{-3}$ g cm^{-2} for the continua from the 4 *S* and 4 *P* levels of Ca II and $m_0 = 5 \times 10^{-3}$ g cm^{-2} for the continua from the 3 *D* levels of Ca II. Deeper in the atmosphere the radiation temperature follows the electron temperature ($T_R = T$), higher up it is supposed to be constant ($T_R = T(m_0)$). We shall discuss the influence of these radiation temperatures on the ionization equilibrium and the line formation in Section 4.

3.4. Absorption and Emission Profiles

As already mentioned, the splitting of the lines due to a magnetic field in sunspots of possibly 2000 to 3000 Gauss will be investigated in a forthcoming study and is not taken into account here. As absorption profile we use the normalized Voigt function

$$\phi(v) = \frac{1}{\sqrt{\pi}} H(a, v), \tag{6}$$

where a and v have their usual meaning.

It was shown by Shine et al. (1975) that a treatment of the Ca II, H and K lines by means of partial redistribution (PRD) is by far better than the assumption of equality of emission and absorption profiles or complete redistribution (CRD). Since PRD strongly influences the wings of the lines and the intensity ratio of the H and K lines we have to use PRD models to study, for example, the position of the K_1 minima. For this purpose we use the formalism by Heasley and Kneer (1976); as suggested by the results of Shine et al. (1975), we treat only the H and K lines with PRD and assume CRD for the IR lines. For simplicity the approximate form of the redistribution function R_{II} by Jefferies and White (1960) is adopted and normalized as proposed by Kneer (1975). Since the complete linearization scheme of Auer and Heasley (1976) does not allow for the linearization of a line source function depending explicitly on the radiation field we lag the PRD calculations behind each linearization cycle, i.e. we only partially linearize the radiative transfer equation. This procedure was recommended by Heasley and Kneer (1976) and it does not deteriorate the convergence properties of the scheme in the case of the Ca II ion.

4. Umbra Models

4.1. Temperature, Electron Density, and Macro-Velocity

In Figures 2 and 3 the run of temperature, electron density, and mass density of four umbra models is given. The corresponding heights are also indicated at the bottom of Figure 2. ($h = 0$ at $\tau_{5000} = 1$.) The temperature model in the deep layers below the 3200 K level is taken from Kneer (1972). The difference between the latter model and models by Hénoux (1969) and Stellmacher and Wiehr (1970) is of little influence on the discussion of models of umbral *chromospheres*. The 3200 K minimum is somewhat uncertain: the available observations of the Ca II lines determine the temperature in these layers within about ± 400 K. Only temperatures below 12 000 K are given. Our actual models extend almost linearly on the logarithmic mass scale to 16 000 K. The chromospheres *A*, *B*, and *C* qualify as optically *thick* in the centre of the K line. Model *D* is optically *thin*. We comment on this below.

Figures 4 and 5 show calculated profiles near the core of the H, K and IR lines at $\cos\theta = 0.89$. The profiles of Figures 4 and 5*a,b,c,d* correspond to the models *A*, *B*, *C*, and *D*, respectively. The micro-velocity used in these calculations (except for Figs. 4*d* and 5*d*) is 1 km s^{-1} throughout the atmosphere; this seems to be an upper limit in the deep layers according to Kjeldseth Moe (1973). (The weakly drawn H and K lines in Fig. 4*d* and the IR lines in Fig. 5*d* are calculated with the micro-velocity of Fig. 7, curve 4.)

Only the thin model *D* produces non-reversed emission cores in H and K. The reason may be seen in Figure 6, which displays the line centre K line source functions and the corresponding Planck function versus τ_{0K} (the

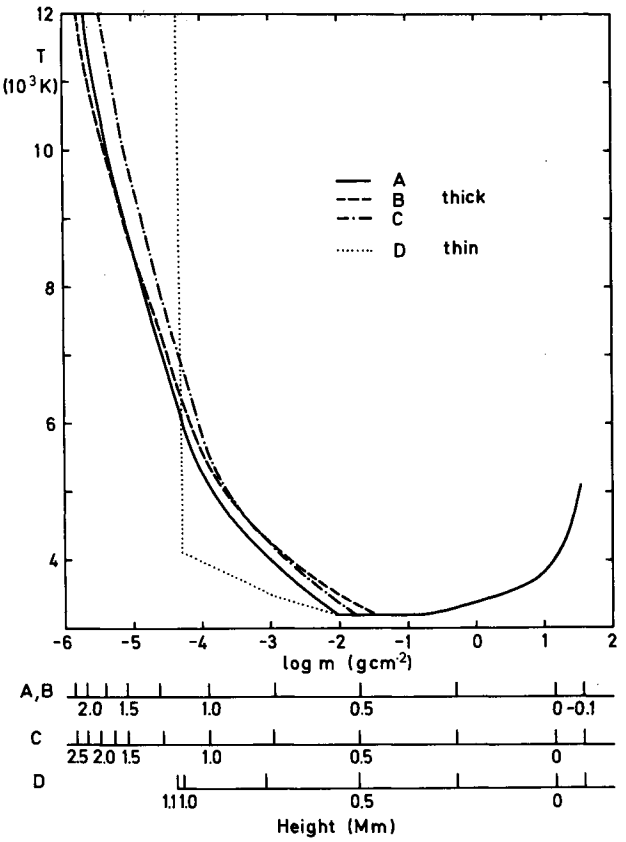

Fig. 2. Temperature versus column mass density for models 1 to 4. Bottom: geometric height for the different models; $h = 0$ at $\tau_{5000} = 1$

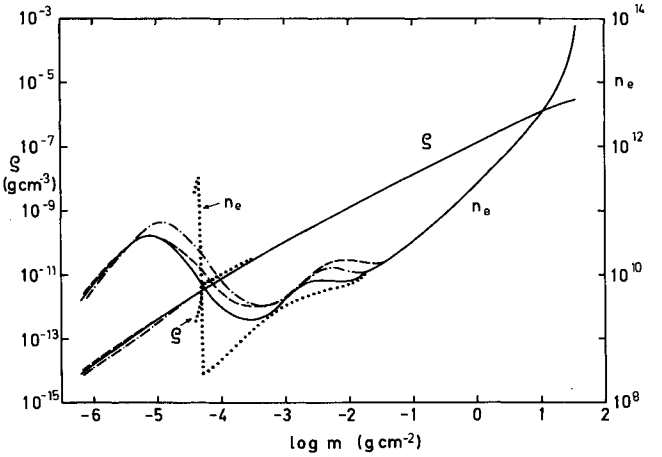

Fig. 3. Electron density (particles per cm³) and mass density versus column mass density for model *A* (full line), *B* (dashed), *C* (dash-dotted), and *D* (dotted)

line centre optical depth in the K line) for the four models. While the thick models have their source function maxima in the range $10 \lesssim \tau_{0K} \lesssim 20$ and so produce self-reversed emission cores, the source function maximum in the thin model is situated where $\tau_{0K} < 1$, leading to a simple emission core.

Athay and Skumanich (1968) suggested that the observed absence of self-reversal in sunspot K line profiles was an indication that the chromosphere above sunspots is optically thin in the K line. Optically thin models are tightly constrained by the requirement that the source function maximum lies where $\tau_{0K} < 1$, i.e. that the main contribution to the emission comes from optically thin layers. This is only possible when there are high electron densities at high temperatures in these layers. The high temperature electrons provide a large thermal source for photons through collisional excitation and subsequent spontaneous radiative emission. In a two-level atom approximation, the total emission E is proportional to the cumulating effect of collisional excitation

$$E \propto \int C_{lu} dn_{\mathrm{Ca\,II},l} \tag{7}$$

where C_{lu} is the collisional rate coefficient from the lower to the upper level and $n_{\mathrm{Ca\,II},l}$ is the density in the ground

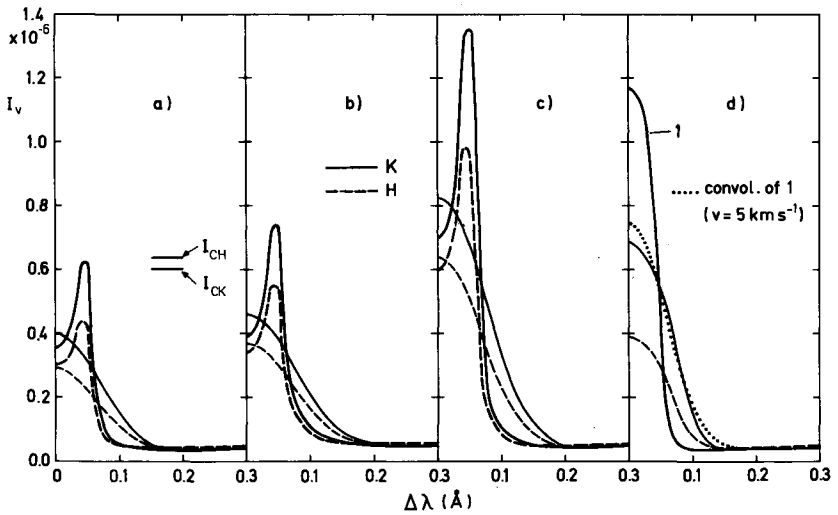

Figs. 4a–d. Emergent intensities of H and K lines at $\cos\theta = 0.89$ in absolute units (erg cm^{-2} s^{-1} sterad^{-1} Hz^{-1}) versus distance from line centre in Å for models *A* (a), *B* (b), *C* (c), and *D* (d). I_c = continuum intensity, equal for all models. (a), (b), and (c): heavily drawn profiles: $v_t = 1$ km s^{-1}; weakly drawn profiles: convolution of heavily drawn profiles with Gaussian distribution corresponding to a velocity amplitude of $v_{\mathrm{macro}} = 5$ km s^{-1}. (d): profile labelled 1: K line, $v_t = 1$ km s^{-1}; dotted: convolution of 1 with Gaussian distribution $v_{\mathrm{macro}} = 5$ km s^{-1}; weak lines: H and K calculated with run of micro-turbulence according to Figure 7, curve 4. Micro- and macro-turbulence have nearly the same effect on the line profiles from the thin model *D*

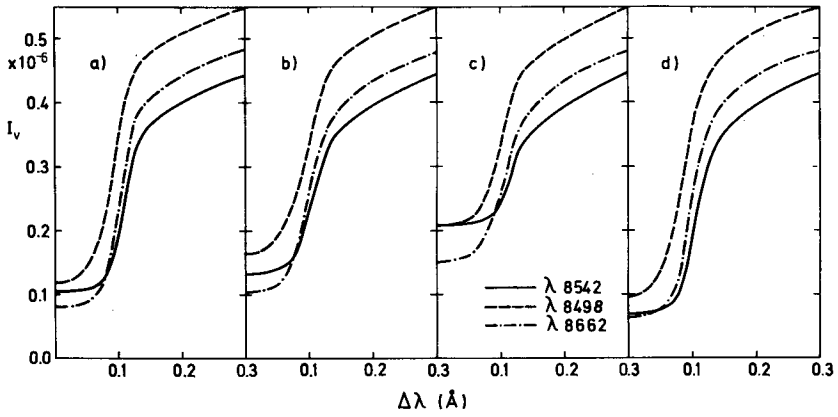

Fig. 5. Emergent intensities of the IR lines at $\cos\theta = 0.89$ in absolute units for the models *A* to *D*. (a)–(c): $v_t = 1$ km s^{-1}; (d) v_t according to curve 4 of Figure 7.

$I_{c\,8542} = 7.53 \times 10^{-6}$ erg cm^{-2} s^{-1} sterad^{-1} Hz^{-1};

$I_{c\,8498} = 7.48 \times 10^{-6}$ erg cm^{-2} s^{-1} sterad^{-1} Hz^{-1};

$I_{c\,8662} = 7.70 \times 10^{-6}$ erg cm^{-2} s^{-1} sterad^{-1} Hz^{-1}

level of Ca II. To the same approximation, the proportionality (7) can be expressed as

$$E \propto \int \varepsilon B d\tau_K \tag{8}$$

where $\varepsilon \approx C_{ul}/A_{ul}$ with the Einstein coefficient A_{ul}, and B is the Planck function. The integral has to be taken over the optically thin emitting layer. Neglecting the coupling collisions between the upper levels of the H and K line transitions, we may apply the same Equation (8) with the same ε and B to the H line except that the latter has half of the opacity of K ($d\tau_H = \frac{1}{2}d\tau_K$). Thus, one would expect an intensity ratio in the emission cores close to 2. The thin model *D* gives $I_{K3}/I_{H3} = 1.77$. Such a large value has been observed only once, by Shine and Linsky (1972). If the electron density and the temperature do not drop *rapidly enough* towards larger optical depths in the *K* line the cumulating effect of thermal sources leads to an increase in the line source function towards larger optical depth, and this produces a self-reversal in the emission.

Thus, except for very special models, thin models will exhibit intensity ratios which are too large, while thick models will exhibit central reversals. It seems improbable that sunspots always produce those special atmospheres (we have not found one) which are thick enough to reduce the intensity ratios, but not too thick to lead to self-reversal. This argument does not rely on the assumption of hydrostatic equilibrium, but only on the run of temperature and electron density with optical depth in *K*.

A *cool* absorbing layer above a *hot* emitting layer, as suggested by Engvold (1966) and Teplitskaja and Firstova (1976) is not necessary to produce an absorption feature in the line centre of *H* and *K*.

It could be argued that the disagreement between the prediction of central absorption features of the optically thick models *A*, *B*, and *C* and the absence of this absorption in most observations is a major objection to the optically thick models. But we do not believe that such a conclusion necessarily follows. We cannot rule out the possibility that the umbral chromosphere *is* optically thick in the K line, and that the self-reversal predicted by our plane-parallel static model is obliterated by the effects of time- and space-dependent dynamical processes on the line profile. The important role of such processes in the formation of the quiet sun K line profile has been discussed by Durrant et al. (1976) and others, and occurrence of dynamical phenomena in umbra chromospheres is well documented (Beckers and Schultz, 1972; Giovanelli, 1972).

We would like to include such effects in our models. Unfortunately, long exposure times and problems with false light prevent the spectroscopic study of non-flashing sunspot fine structure, and there are presently no theories for umbral dynamics which are developed to the point of predicting the parameters we need for a line formation study. In the absence of both theoretical and observational guidelines we cannot construct a detailed dynamical model and then compute a spatially averaged profile for comparison with the observations. To illustrate what could occur, however, we have convolved the theoretical profiles with a Gaussian macro-turbulence profile of 5 km s^{-1} amplitude. As can be seen from

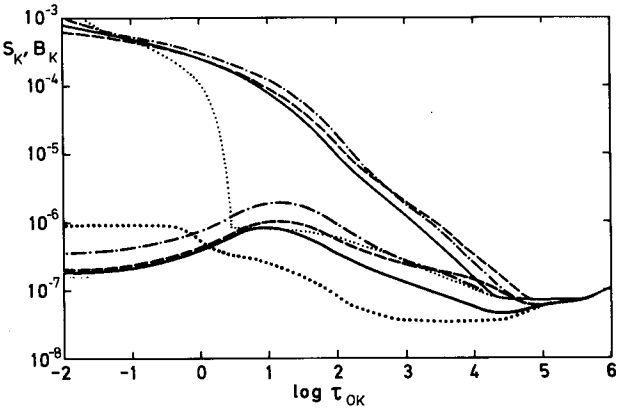

Fig. 6. Line centre source function of K line (heavily drawn) and Planck function (weakly drawn) versus optical depth of K line centre for model *A* (full line), *B* (dashed), *C* (dash-dotted), and *D* (dotted). Thick atmospheres (*A*–*C*) have the source function maximum at $\tau_{0K} > 1$, thin atmospheres (*D*) at $\tau_{0K} < 1$

Figure 4, this completely removes the self-reversal in the optically thick models. There is no physical basis for the amplitude or even the form of the macro-turbulence and, consequently, there is little point in comparing the smeared profiles with the observations. However, this velocity model illustrates the possibility that dynamical processes in optically thick umbral chromospheres could lead to unreversed profiles. We might mention that theoretical non-LTE emission line profiles almost always exhibit central absorption features deeper than those of the corresponding observations (e.g. quiet sun K line; Ayres, 1975; plage K line; Shine and Linsky, 1974). In these cases too, dynamical processes could be responsible for the disparity.

When comparing the optically thick models differentially we notice two effects. First, in going from model *A* to model *B*, the overall increase in emerging intensities is small. But the ratio I_{K3}/I_{H3} of the Gaussian convolved profiles, which is now a measure of the ratio of the *total* emission in H and K, decreases from 1.38 to 1.24. This is due to the deeper onset of the chromospheric temperature rise in model *B*. Second, in going from model *A* to model *C*, we see large increases in the emergent core intensities because of the overall increase of temperature and electron density. The λ8542 line exhibits a trace of line centre emission in model *C*.

4.2. *Micro-Velocities and Radiation Temperatures*

We investigate first the influence of the run of the micro-velocity on the K line profile and then the effect of varying the radiation temperatures in the Balmer continuum and in the ionizing continua of Ca II, which cause some uncertainties in both the atmospheric models and the Ca II ionization equilibrium. For these test calculations we use the thick atmospheric model *A* of Figures 2 and 3, a three-level plus continuum model atom for Ca II, and treat the radiative transfer with CRD. The computational simplifications do not invalidate the conclusions drawn from differential trends.

Figure 7 gives several curves for the micro-velocities. (Curve 4 was designed for the thin model.) As already mentioned, a micro-velocity of $v_t = 1$ km s^{-1} seems to be an upper limit at large depths (Kjeldseth Moe, 1973). Above sunspots, at levels of the transition zone to the corona, Cheng et al. (1976) observe an *increase* with height (temperature) of the non-thermal broadening. Their measured value of 9 km s^{-1} at the 16 000 K level is also included in Figure 7. A *decrease* of the Doppler broadening with height, as suggested by Teplitskaja and Efendieva (1975), does not fit easily to the above boundary values. Therefore we have not included such a run of micro-velocities in our calculations. Figure 8*a* shows the resulting profiles of the K line. The bigger the micro-velocity the broader is the line profile and the less pronounced is the self-reversal. We cannot, however, force the self-reversal to disappear for reasonable values of the micro-turbulence.

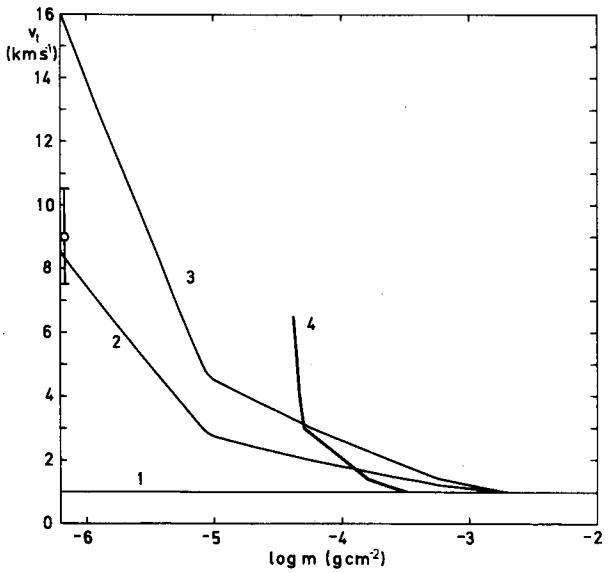

Fig. 7. Several runs of micro-turbulence. Curve 4 is used only for the thin model *D*. Φ: non-thermal broadening at the 16 000 K level measured by Cheng et al. (1976)

Figure 8*b* shows the differential effects on the K line of different ionizing radiation temperatures. If we assume that the Balmer continuum radiation temperature is only 3000 K instead of the reference value 3500 K the hydrogen ionization in the chromosphere is reduced. As a result of the smaller electron density the source function and the emergent intensity of the K line is weakened (profile 2 in Fig. 8*b*). On the other hand, if we assume a higher temperature than the usual $T_R < 4000$ K for the ionization continua of Ca II (this could be produced, for example, if there were many strong emission lines below 1500 Å) the ionization equilibrium is shifted in favour of Ca III. This reduces the optical thickness of the high temperature chromosphere and weakens the emission of the K line (Fig. 8*b*, profile 3).

4.3. *A Model*

One of the aims of this study is to use the Ca II spectrum to provide a reference model for the chromosphere above sunspots. We are inclined to reject a thin model: it appears to be easier to account for the failure of most observations to reveal the self-reversal predicted by the thick model than to account for the line intensity ratio predicted by a thin model. We propose as reference model the thick model *C* of Figures 2 and 3, together with the run of micro-turbulence of curve 2 in Figure 7. The emergent line profiles are shown in Figure 9. The theoretical K line closely resembles the profiles observed by Engvold (1967). After smoothing of the self-reversed

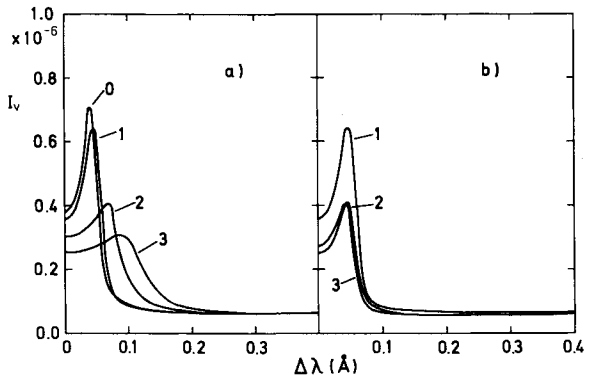

Fig. 8a. Effect of different micro-velocities on the K line emission core in model A, $\cos\theta = 0.89$. Label 0: $v_t = 0$ km s^{-1}; labels 1–3; curves 1–3 of Figure 7. **b** Effect of different radiation temperatures in the ionization continua. Label 1: $T_{R,B} = 3500$ K; $T_{R,4S\text{-cont}} =$. 3900 K; $T_{R,4P\text{-cont.}} = 3400$ K;
Label 2: $T_{R,B} = 3000$ K; others the same as for 1
Label 3: $T_{R,B} = 3500$ K; $T_{R,4S} = T_{R,3D} = T_{R,4P} = 5500$ K.
Profiles in (a) and (b) from a three-level plus continuum model atom and with complete redistribution

emission cores of the H and K lines by a Gaussian distributed macro-velocity with 5 km s^{-1} amplitude the profiles exhibit closely the features reported by the other investigators as listed in Table 1. The ratio $I_{K3}/I_{H3} \approx 1.18$ lies well in the observed range. The K_1 position is mainly a function of the non-thermal velocities. The wing beyond K_1 is extremely flat. The IR lines also fulfill the requirements of Table 1.

We compare our reference model with the quiet chromosphere model of Vernazza et al. (1973) and the umbra model of Baranovski (1974) in Figure 10. We have tried the latter model and have found that with the abundance of Ca used here the K line emission is too strong by factors five to ten. The temperature and electron density seem to be too high in the upper layers of Baranovski's model.

At the 16 000 K level, our model possesses a pressure of 0.03 dyn cm^{-2}, which is five times smaller than the coronal pressure above the quiet chromosphere, and an electron density of 6×10^9 cm^{-3}, which is four times lower than the value estimated by Cheng et al. (1976) for the 36 000 K level above umbrae. The temperature gradient in the top layers is about 8 K km^{-1}.

5. Conclusion

We have presented a model of the chromosphere above sunspots which can explain many aspects of the observed emission features in the Ca II, H and K lines and the IR lines of Ca II. To explain the line centre intensity ratio of K and H, which is close to unity, we have chosen an optically thick chromosphere. Such a model exhibits self-reversals in H and K line cores which are rarely observed (Engvold, 1967).

We can suggest several possible explanations of this problem. First, we should wait for a treatment of the non-LTE radiative transfer problem in the presence of magnetic fields. The emission features of H and K are expected to be broadened by the Zeeman-splitting. Second, spectrograms of the best available resolution in wavelength, space and time should reveal if the H and K lines exhibit self-reversed profiles characteristic of an optically thick atmosphere on very small scales. Third, macroscopic velocities such as those observed by Giovanelli (1972) could change the asymmetric doubly peaked profiles predicted by thick models into asymmetric single emission peaks as a result of differential velocity fields, just as in the quiet chromosphere. (See e.g. Durrant et al., 1976.) This effect should be studied both observationally and theoretically. Finally, we do not claim uniqueness for our umbra model. Possibly, there exists a *static* model which gives pure emission cores with the correct intensities (and intensity ratios). However, this would probably be a very special model and unlikely to be realized in all the different kinds of umbrae. We feel that a search for such a model is unwarranted, in view of the many observational uncertainties and of the other possible explanations.

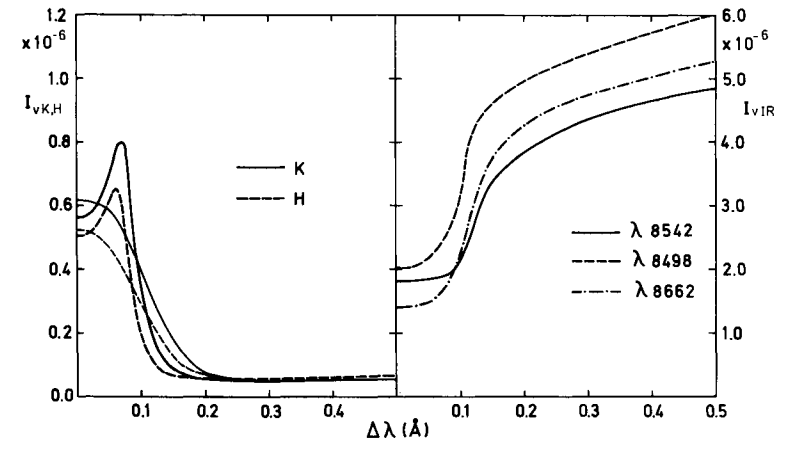

Fig. 9. Profiles of the Ca II lines emitted from the suggested umbra chromosphere model, $\cos\theta = 0.89$. H and K are again convolved with a Gaussian profile with an amplitude of 5 km s^{-1} (weak lines)

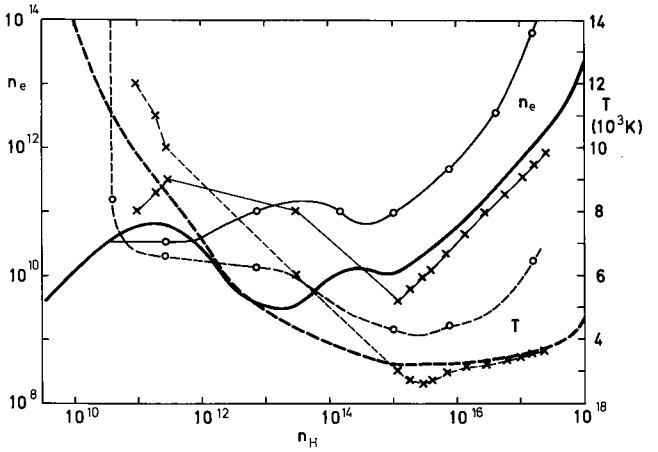

Fig. 10. Electron number density (full lines) and temperature (dashed lines) versus hydrogen number density. Heavy lines: suggested umbra model; crosses: umbra model of Baranovski (1974); open circles: *photospheric* model of Vernazza et al. (1973)

We consider the umbra model presented above as a starting point for further investigations. It should be checked and improved with additional observations, including lines and continua in the far ultra-violet spectral region. We have already mentioned the pressing need for high quality observations of the Ca II infra-red triplet. The model is also intended as a guide for magneto-dynamic considerations which treat the energy balance in umbral chromospheres. Our model may help answer the question of the distribution of energy dissipation in sunspots.

Appendix

A.1. The Ionization of Hydrogen

We have to clarify the meanings of ε_0 and G in Equation (5):

$$\varepsilon_0 = \frac{C_{1K}}{R_{K1}}\left[1 + \frac{C_{12}(1 + C_{2K}/R_{K2})/(R_{2K}/R_{K2})}{C_{1K}(1 + C_{2K}/R_{2K} + C_{21}/R_{2K})}\right], \quad \text{(A.1)}$$

$$G = \frac{1 + (C_{12}/C_{1K})(R_{2K} + C_{2K})/(R_{2K} + C_{2K} + C_{21})}{1 + (C_{12}/C_{1K})(R_{K2} + C_{2K})/(R_{2K} + C_{2K} + C_{21})}. \quad \text{(A.2)}$$

Linsky (1968) gives slightly different formulae. However, a close inspection of the steady state rate equations (Mihalas 1970) and of the procedure of Dietz and House (1965) convinces us that the expressions (A.1) and (A.2) are appropriate. The C_{ij}'s represent collisional rate coefficients proportional to the electron density with

$$C_{ij} = n_e\Omega_{ji}(T)\exp(-h\nu_{ij}/kT), \quad (j > i) \quad \text{(A.3)}$$

and

$$C_{ji} = n_e\Omega_{ji}(T)g_i/g_j \quad \text{(A.4)}$$

where the g's are the statistical weights. For Ω_{ji} we choose values independent of temperature from a table by Avrett (1974)

$$\Omega_{21} = 2.5 \times 10^{-8}$$

$$\Omega_{K1} = 3.0 \times 10^{-9}$$

$$\Omega_{K2} = 1.0 \times 10^{-7}.$$

For the radiative rate coefficients we neglect stimulated emission and have the formulae

$$R_{Ki} = 4\pi\int_{\nu_{iK}}^{\infty}\frac{\alpha_i(\nu)}{h\nu}\frac{2h\nu^3}{c^2}\exp(-h\nu/kT)d\nu, \quad (i = 1, 2) \quad \text{(A.5)}$$

and

$$R_{2K} = 4\pi w\int_{\nu_{2K}}^{\infty}\frac{\alpha_2(\nu)}{h\nu}B_\nu(T_{R,B})d\nu, \quad \text{(A.6)}$$

where $B_\nu(T_{R,B})$ is the Planck function at the radiation temperature of the Balmer continuum $T_{R,B}$ and w is the dilution factor. For the frequency dependence of the absorption cross-sections we take

$$\alpha_i(\nu) = \alpha_{i0}\left(\frac{\nu_{iK}}{\nu}\right)^3, \quad (i = 1, 2) \quad \text{(A.7)}$$

and from Allen (1973) at the head of the continua ($\nu = \nu_{iK}$) we have

$$\alpha_{i0} \approx 7.9 \times 10^{-18} \times i. \quad \text{(A.8)}$$

In Equation (A.8) we set the Gaunt factors equal to unity.

A.2. Atomic Data of Ca II

The data given below are mostly interpolations and simplifications of the set of atomic data compiled by Shine and Linsky (1974). We feel that such simplifications are justified in view of the preliminary nature of our model calculations and of the many observational uncertainties.

Table A.1 summarizes the data used. The abundance of Ca is taken from Shine et al. (1975). The ionization frequencies and statistical weights of the levels as well as the wavelengths, oscillator strengths (or continuous absorption coefficients) for radiative transitions are given. The definition of the α_{i0}'s is the same as in Equation (A.7). For the collisional rate coefficients we use the expression (A.3) with a temperature dependence according to

$$\Omega_{Ki}(T) = CE_{Ki} \times \sqrt{T} \quad \text{(A.9)}$$

for the ionizing collisions and

$$\Omega_{ji}(T) = CE_{ji}/\sqrt{T}, \quad (j > i) \quad \text{(A.10)}$$

for the bound-bound collisions. Values of CE_{ji} are given in Table A.1. Collisions by neutral hydrogen atoms are neglected.

Table A.1

Abundance 2.14×10^{-6}						
Level Parameters						
Level	1	2	3	4	5	6 (cont.)
Term	$4s^2S_{1/2}$	$3d^2D_{3/2}$	$3d^2D_{5/2}$	$4p^2P_{1/2}$	$4p^2P_{3/2}$	$4s^2p^6{}^1S_0$
Designation						
Ionization Frequency (10^{15} Hz)	2.87158	2.46211	2.46029	2.11601	2.10933	0.0
g	2	4	6	2	4	1
Radiative Transitions						
Transition	5–1	5–2	5–3	4–1	4–2	
λ (Å)	3934	8498	8542	3968	8662	
f	0.66	0.00883	0.053	0.33	0.0442	
Transition	6–1	6–2	6–3	6–4	6–5	
λ (Å)	1044	1218	1219	1417	1422	
α_{i0} (10^{-18} cm^2)	0.22	6.2	6.2	2.4	2.4	
Collisional Transitions						
Transition	5–1	5–2	5–3	5–4	4–1	
CE	4.1 (−5)	2.1 (−5)	6.5 (−5)	4.3 (−5)	2.1 (−5)	
Transition	4–2	4–3	3–1	3–2	2–1	
CE	4.9 (−5)	0.44 (−5)	3.6 (−5)	4.6 (−5)	2.4 (−5)	
Transition	6–1	6–2	6–3	6–4	6–5	
CE	1.45 (−10)	1.88 (−10)	1.88 (−10)	2.68 (−10)	2.68 (−10)	

The damping constant of the Voigt profile, Equation (6), is represented by

$$a = (\Gamma_R + \Gamma_{VW} n_H)/4\pi\Delta\nu_D \qquad (A.11)$$

where n_H is the number density of neutral hydrogen and $\Delta\nu_D$ the Doppler width. For all lines we use a radiative damping width of

$$\Gamma_R = 1.5 \times 10^8 \text{ s}^{-1}$$

and a Van der Waals broadening constant of

$$\Gamma_{VW} = 1.6 \times 10^{-8} \text{ cm}^3 \text{ s}^{-1}.$$

Acknowledgements. We wish to express our deepest gratitude to Drs. L. H. Auer and J. N. Heasley for their invaluable support with the difficult calculations. It is a pleasure to thank Dr. L. E. Cram for discussions and helpful comments during the preparation of the manuscript. The calculations were carried out on the UNIVAC 1106 computer of the Rechenzentrum der Universität Freiburg.

References

Allen, C. W.: 1973, Astrophysical Quantities, 3rd edition, Athlone Press, p. 96
Athay, R. G., Skumanich, A.: 1968, *Solar Phys.* **3**, 181
Auer, L. H., Heasley, J. N.: 1976, *Astrophys. J.* **205**, 165
Auer, L. H., Heasley, J. N., House, L. L.: 1977, *Astrophys. J.* **216**, 531
Auer, L. H., Heasley, J. N., Milkey, R. W.: 1972, Kitt Peak National Observatory Contribution No. 555
Avrett, E. H.: 1974, private communication
Ayres, T. R.: 1975, Ph.D. thesis, University of Colorado
Baranovski, E. A.: 1974, *Izv. Krymsk. Astrofiz. Obs.* **51**, 56
Beckers, J. M.: 1976, *Astrophys. J.* **203**, 739
Beckers, J. M., Schultz, R. B.: 1972, *Solar Phys.* **27**, 61
Beckers, J. M., Tallant, P. E.: 1969, *Solar Phys.* **7**, 351
Biermann, L.: 1941, *Vierteljahresschr. Astron. Gesellsch.* **76**, 194
Burgess, A.: 1965, *Smithsonian Special Report* **174**, 47
Cheng, C.-C., Doschek, G. A., Feldman, A.: 1976, *Astrophys. J.* **210**, 836
Danielson, R. E., Savage, B. D.: 1968, *IAU Symp.* **35**, (Kiepenheuer ed.), 112
Dietz, R. D., House, L. L.: 1965, *Astrophys. J.* **141**, 1393
Durrant, C. J., Grossmann-Doerth, U., Kneer, F.: 1976, *Astron. Astrophys.* **51**, 95

Engvold, O.: 1966, *Astrophysica Norvegica* **10**, 101
Engvold, O.: 1967, *Solar Phys.* **2**, 234
Foukal, P.V., Huber, M.C.E., Noyes, R.W., Reeves, E.M., Schmahl, E.J., Timothy, J.G., Vernazza, J.E., Withbroe, G.L.: 1974, *Astrophys. J. Letters* **193**, L143
Gingerich, O., Noyes, R.W., Kalkofen, W., Cunny, Y.: 1971, *Solar Phys.* **18**, 347
Giovanelli, R.G.: 1972, *Solar Phys.* **27**, 71
Heasley, J.N., Kneer, F.: 1976, *Astrophys. J.* **203**, 660
Hénoux, J.C.: 1969, *Astron. Astrophys.* **2**, 288
House, L.L., Steinitz, R.: 1975, *Astrophys. J.* **195**, 235
Jefferies, J.T., White, R.O.: 1960, *Astrophys. J.* **132**, 767
Kjeldseth Moe, O.: 1973, *Solar Phys.* **33**, 393
Kneer, F.: 1972, *Astron. Astrophys.* **18**, 39
Kneer, F.: 1975, *Astrophys. J.* **200**, 367
Labs, D., Neckel, H.: 1968, *Z. Astrophys.* **69**, 1
Linsky, J.L.: 1968, *Smithsonian Special Report.* **274**
Linsky, J.L.: 1970, *Solar Phys.* **11**, 355
Linsky, J.L., Avrett, E.H.: 1970, *Publ. Astron. Soc. Pacific* **82**, 169
Marik, M.: 1967, *Soviet Astron.—AJ* **11**, 264
Mattig, W., Kneer, F.: 1977, *Astron. Astrophys.*
Mihalas, D.: 1970, *Stellar Atmospheres*, Freeman, San Francisco, p. 144
Mustel, E.R., Tsap, T.T.: 1960, *Izv. Krymsk. Astrofiz. Obs.* **22**, 75
Omont, A., Smith, E.W., Cooper, J.: 1973, *Astrophys. J.* **182**, 283
Parker, E.N.: 1974, *Solar Phys.* **36**, 249
Shine, R.A., Linsky, J.L.: 1972, *Solar Phys.* **25**, 357
Shine, R.A., Linsky, J.L.: 1974, *Solar Phys.* **39**, 49
Shine, R.A., Milkey, R.W., Mihalas, D.: 1975, *Astrophys. J.* **199**, 724
Stellmacher, G., Wiehr, E.: 1970, *Astron. Astrophys.* **7**, 432
Teplitskaja, R.B., Efendieva, S.A.: 1971, *Soln. Dannye* **3**, 80
Teplitskaja, R.B., Efendieva, S.A.: 1973, *Solar Phys.* **28**, 369
Teplitskaja, R.B., Efendieva, S.A.: 1975, *Solar Phys.* **43**, 293
Teplitskaja, R.B., Firstova, N.M.: 1976, *Solar Phys.* **48**, 103
Vernazza, J.E., Avrett, E.H., Loeser, R.: 1973, *Astrophys. J.* **184**, 605
White, R.O., Suemoto, Z.: 1968, *Solar Phys.* **3**, 523
Zwaan, C.: 1965, *Rech. Astron. d'Utrecht* **17**, part 4